Universitat Autònoma de Barcelona

Master Thesis

Veneziano amplitudes for the light-by-light scattering

Author:
Aleix López

Supervisor:
Dr. Pere Masjuan

A thesis submitted in fulfilment of the requirements for the Postgraduate Program

in

High Energy Physics, Astrophysics and Cosmology
Institut de Física d'Altes Energies

September 4, 2018

Declaration of Authorship

I, Aleix López, declare that this thesis titled, "Veneziano amplitudes for the light-by-light scattering" and the work presented in it are my own. I confirm that:

- This work was done wholly or mainly while in candidature for a research degree at this University.
- Where any part of this thesis has previously been submitted for a degree or any other qualification at this University or any other institution, this has been clearly stated.
- Where I have consulted the published work of others, this is always clearly attributed.
- Where I have quoted from the work of others, the source is always given. With the exception of such quotations, this thesis is entirely my own work.
- I have acknowledged all main sources of help.
- Where the thesis is based on work done by myself jointly with others, I have made clear exactly what was done by others and what I have contributed myself.

Signed:

Date:

UNIVERSITAT AUTÒNOMA DE BARCELONA

Abstract

High Energy Physics, Astrophysics and Cosmology
Institut de Física d'Altes Energies

Master Thesis

Veneziano amplitudes for the light-by-light scattering

by Aleix López

The anomalous magnetic moment of the muon a_μ induced by the pseudoscalar-pole contribution to the hadronic light-by-light scattering is considered using a description of the $\pi^0\gamma\gamma$, $\eta\gamma\gamma$ and $\eta'\gamma\gamma$ transition form factors in the pion-pole approximation based on the Dual-Large N_c QCD model. This framework improves considerably the VMD and LMD results by summing up all the infinite number of zero width resonances that appear in the large-N_c limit, with masses and couplings fixed so that the form factors become Euler Beta functions of the Veneziano type. The resulting two-loop integrals are treated by first performing the angular integration analytically, using the method of Gegenbauer polynomials, followed by a numerical evaluation of the remaining two-dimensional integration over the moduli of the Euclidean loop momenta. The results obtained $a_{\mu\ EVMD}^{LbL;PS} = (6.2 \pm 1.2) \times 10^{-10}$ and $a_{\mu\ ELMD}^{LbL;PS} = (7.3 \pm 1.2) \times 10^{-10}$ are below the average. Complementing these results with those from the "Glasgow consensus" we have obtained the discrepancies $\Delta a_\mu^{EVMD} \approx 4.4\sigma$ and $\Delta a_\mu^{ELMD} \approx 4.3\sigma$, which substantially increase the discrepancy of $3-4\sigma$ between experiment and theory that has been obtained from the most recent models and data. Therefore, it is a sign of New Physics more promising than before.

Contents

Chapter 1

Introduction

The anomalous magnetic moment of the muon a_μ is one of the most accurately measured quantities in particle physics [49]. The high precision of measurement, as well as theoretical prediction, renders a_μ a very promising signal of new physics if a deviation from its prediction in the Standard Model (SM) is found.

a_μ is sensitive to all three interactions of the Standard Model. The most commonly known of them is the electromagnetic interaction, described by Quantum Electrodynamics (QED). It can be treated perturbatively and is calculated straight forward. The impact of the weak force is small but traceable. However, the strong force, described by Quantum Chromodynamics (QCD), yields considerable contributions to a_μ and due to the non-perturbative nature of QCD, the calculation of its physics is quite involved. That is why the largest uncertainties in the SM prediction come from the leading hadronic contributions: the hadronic vacuum polarization and the hadronic light-by-light scattering insertions. In order to compute them, most groups resort to effective field theories that use, e.g. mesons as degrees of freedom [33].

a_μ^{exp} measured by Brookhaven National Laboratory (BNL) E821 experiment represents an interesting but not yet conclusive 3.4 sigma discrepancy from the Standard Model prediction (a_μ^{SM}) [64]. The latest E821 measurement was performed in 2001, but the two next generation muon $g-2$ experiments at Fermilab in the US and at J-PARC in Japan have been designed to reach a four times better precision of 16×10^{-11} (from 0.54 ppm to 0.14 ppm) and expects to collect 21 times the E821 statistics [40]. The first and the last results are expected to release in 2018 and 2020 respectively. If the precision is improved and the central value stays unchanged, the difference between theory and experiment will rise up to 7.5 standard deviations. This could be an even clearer sign of new physics beyond the Standard Model (BSM).

The structure of the thesis is as follows: In the remains of this chapter, we proceed to give a general overview of the basic concepts of the magnetic moment of the muon. We describe the experimental extraction method and put special emphasis on the Fermilab E989 experiment. We make a compilation of the contributions present in the Standard Model and give a synopsis of the current values of said contributions. Then, we discuss very briefly the discrepancy $a_\mu^{\text{exp}}-a_\mu^{SM}$ and the many interpretations of BSM that could handle with it.

In chapter 2 we present our framework. It elaborates on general aspects of the hadronic light-by-light contribution to a_μ and the full rank hadronic vacuum polarization tensor $\Pi_{\mu\nu\lambda\rho}$. We explain the steps we took to extract the anomalous magnetic moment. We focus on the pion-pole contribution using the method of Gegenbauer polynomials. Then, we present our calculations of the transition form factor and the electromagnetic form factor in the framework of Dual-Large N_c QCD (Dual-QCD$_\infty$).

In chapter 3 we present the results of the thesis and discuss its behaviour. We compare our findings with those of other references.

A short summary and conclusion of the thesis is given in chapter 5, as well as future directions in this line of work.

1.1 The anomalous magnetic moment

Consider the Pauli equation. This is the Schrödinger equation for spin-1/2 particles, which takes into account the interaction of the particle's spin with an external electromagnetic field. It is the non-relativistic limit of the Dirac equation.

$$i\hbar\frac{\partial\hat{\varphi}}{\partial t} = \hat{\mathbf{H}}\hat{\varphi} = \left[\frac{1}{2m}(\mathbf{p} - e\mathbf{A})^2 + e\Phi - \frac{e\hbar}{2m}\boldsymbol{\sigma}\cdot\mathbf{B}\right]\hat{\varphi} \tag{1.1}$$

where

$$\psi = \hat{\psi}e^{-i\frac{mc^2}{\hbar}t} \quad \text{and} \quad \hat{\psi} = \begin{bmatrix} \hat{\varphi} \\ \hat{\chi} \end{bmatrix} \tag{1.2}$$

are Dirac four-spinors, $\hat{\varphi}$ is a Pauli two-spinor, m is the mass of a particle, e is its electric charge, $\boldsymbol{\sigma}$ are Pauli matrices collected into a vector, $\mathbf{B} = \boldsymbol{\nabla}\times\mathbf{A}$ is an external magnetic field, and Ψ and A are scalar electric and vector magnetic potential respectively [40]. The last term, which presents potential energy of a magnetic dipole in an external field, is the one we are interested in. It has the form of a magnetic interaction Hamiltonian $-\boldsymbol{\mu}\cdot\mathbf{B}$, so we can define the particle's intrinsic magnetic dipole moment

$$\boldsymbol{\mu} = \frac{e\hbar}{2m}\boldsymbol{\sigma} = \frac{e}{m}\mathbf{S}; \quad \mathbf{S} = \hbar\boldsymbol{s} = \hbar\frac{\boldsymbol{\sigma}}{2} \tag{1.3}$$

where $\mathbf{S}$ is the spin angular momentum and $\mathbf{s}$ is the spin quantum number. For comparison, the orbital magnetic moment is

$$\boldsymbol{\mu}_{\text{orbital}} = \frac{e}{2m}\mathbf{L} = g_{\text{l}}\frac{e}{2m}\mathbf{L}; \quad \mathbf{L} = \mathbf{r}\times\mathbf{p} = \hbar\mathbf{l} \tag{1.4}$$

where $\boldsymbol{L}$ is the orbital angular momentum. Now we can construct the total magnetic moment

$$\boldsymbol{\mu}_{\text{total}} = \frac{e}{2m}\left(g_{\text{l}}\mathbf{L} + g_{\text{s}}\mathbf{S}\right) = \frac{m_e}{m}\mu_{\text{B}}\left(g_{\text{l}}\mathbf{l} + g_{\text{s}}\mathbf{s}\right) \tag{1.5}$$

where g_{l} and g_{s} are the orbital and spin g-factors (gyromagnetic ratios) respectively and

$$\mu_{\text{B}} = \frac{e\hbar}{2m_e} \tag{1.6}$$

is the Bohr's magneton. If we consider a lepton and thus use negative electric charge, then also g_{l} and g_{s} are actually negative, $g_{\text{l}} = -1$ and $g_{\text{s}} = -2$. The latter is the famous result, which we get from Dirac or Pauli equation $g_\ell^{(0)} = 2$, but in the framework of quantum field theory (QFT), the value is slightly exceeding 2 (for a detailed discussion see [39, 40]).

If we neglect electrical fields, the quantum correction can be represented with a single number, the anomalous magnetic moment, defined as

$$a_\ell \equiv \frac{g_\ell - 2}{2}, \quad (\ell = e, \mu, \tau) \tag{1.7}$$

which we can get as a result of radiative corrections (RC) or sometimes called relativistic quantum fluctuations. We could say that the gyromagnetic ratio of a lepton is defined as the ratio of the magnetic moment and the spin operator in units of

$\mu_0 = e\hbar/2m_\ell$

$$\boldsymbol{\mu} = g_\ell \frac{e\hbar}{2m_\ell}\boldsymbol{s}; \quad g_\ell = 2\,(1 + a_\ell)\,. \tag{1.8}$$

From the last equation, we can easily distinguish between the tree level part and the anomalous part.

As we can observe from equation (1.7), the anomalous magnetic moment of a lepton a_ℓ is a dimensionless quantity. If we use the most precise determination of the fine structure constant α, which does not depend on a_e, to calculate the theoretical prediction of the electron anomalous magnetic moment (a_e^{SM}), we see that the latter is in good agreement with the recent extraordinary precise measurement a_e^{exp} [40]. a_μ^{exp} represents, unlike a_e, an interesting but not yet conclusive 3.4 sigma discrepancy from the Standard Model prediction a_μ^{SM}. The higher the mass of the lepton, the more sensitive to BSM is its anomalous magnetic moment. This sensitivity to new physics scales with $(m_\ell/\Lambda)^2$ where Λ is the scale of new physics. While a_e is not so interesting, even though it requires to push QED calculations to higher orders, a_μ is much more attractive due to the BSM sensitivity ratio $(m_\mu/m_e)^2 \approx 43000$. It is sensitive to all kinds of effects, and thus forces theorists to predict new theories of physics beyond the Standard Model (see Sect. 1.4.1). If a precise measurement of the τ magnetic moment would be available, the resulting anomality would be even better suited to investigate anomalous contributions to the magnetic moment [33].

In this thesis, we are going to focus on the anomalous magnetic moment of the muon a_μ. The muon's magnetic moment is illustrated as a Feynman diagram in Fig. 1.1(a). This diagram shows the muon coupling directly to a photon from the external magnetic field; it corresponds to the Dirac equation's prediction that $g_\mu^{(0)} = 2$. However, there is a large set of radiative corrections; these couplings to virtual fields lead to the anomalous part a_μ of the magnetic moment. These corrections are represented symbolically by the "blob" in Fig. 1.1(b); any allowed intermediate state may be inserted in its place. We will discuss the contributing effects in Sect. 1.3.

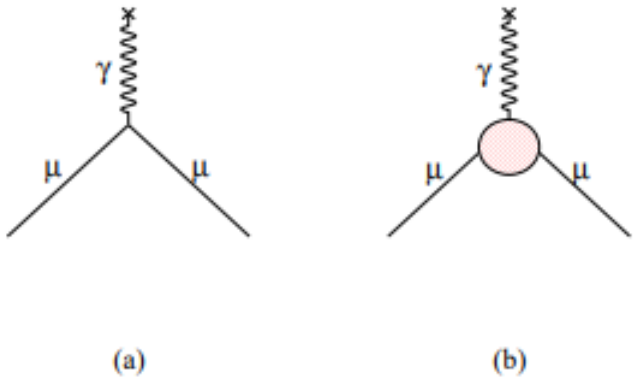

FIGURE 1.1: Feynman diagrams for (a) the magnetic moment corresponding to $g_\mu^{(0)} = 2$, (b) the general form of diagrams that contribute to the anomalous magnetic moment a_μ.

1.2 Experiment

The anomalous magnetic moment of the muon a_μ was measured in three experiments at CERN (CERN I, CERN II and CERN III) between 1961 and 1976 and in the E821 experiment at Brookhaven National Laboratory (BNL) between 1997 and 2001 [40]. Now, new experiments are on the way: one at Fermilab (E989) [28] in the US and another one at J-PARC (E34) [65] in Japan. While the Fermilab experiment represents a major upgrade of the Brookhaven experiment operating with ultra relativistic muons (as the later CERN experiments), the J-PARC experiment is planned to use ultra cold muons and will be the first precise experiment using a very different approach with rather different systematics.

The CERN, E821 and E989 experiments use the same principles: The study of the orbital and spin motion of highly polarized muons in a magnetic storage ring. In this section we are going to describe this mechanism and put special emphasis on the E989 experiment, which is the most improved of all of them.

The experiment proceeds as follows: a collection of longitudinally polarized muons is injected into a storage ring where they follow a circular central orbit in a magnetic dipole field $\boldsymbol{B}$ and a vertically focusing electric quadrupole field $\boldsymbol{E}$ [29]. In the horizontal plane of the orbit the muons execute relativistic cyclotron motion with angular frequency ω_c. On the other hand, the muons carry spin and thus a magnetic moment which is directed along the direction of the flight axis. By the motion of the muon magnetic moment in the homogeneous magnetic field, the spin axis is changed in a particular way as described by the Larmor precession. After each circle the muon's spin axis changes by 12' (arc seconds), while the muon is travelling at the same momentum (see Fig. 1.2). The muon spin is precessing with angular frequency ω_s, which is slightly bigger than ω_c by the difference called angular frequency $\omega_a = \omega_s - \omega_c$.

$$\omega_c = \frac{eB}{m_\mu \gamma} \tag{1.9}$$

$$\omega_s = \frac{eB}{m_\mu \gamma} + a_\mu \frac{eB}{m_\mu} \tag{1.10}$$

$$\omega_a = a_\mu \frac{eB}{m_\mu} \tag{1.11}$$

where $a_\mu = (g_\mu - 2)/2$ is the muon anomaly, γ is the relativistic Lorentz factor and v the muon velocity. Note that if the muon would just have its Dirac magnetic moment $g_\mu^{(0)}$ (tree level) the direction of the spin of the muon would not change at all [40].

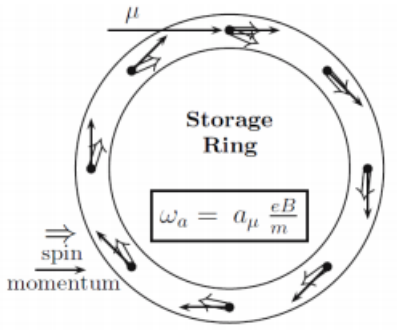

FIGURE 1.2: Spin precession in the storage ring plane.
Adapted from [40].

As we have said, in addition to the magnetic field $\boldsymbol{B}$ an electric quadrupole field $\boldsymbol{E}$ in the plane normal to the particle orbit is applied in order to retain the muons in the ring. This field, modifies ω_a to

$$\boldsymbol{\omega}_a = \frac{e}{m_\mu}\left(a_\mu \boldsymbol{B} - \left[a_\mu - \frac{1}{\gamma^2 - 1}\right]\boldsymbol{v} \times \boldsymbol{E}\right) \tag{1.12}$$

Interestingly, one has the possibility to choose γ such that $a_\mu - 1/(\gamma^2 - 1) = 0$, in which case ω_a becomes independent of $\boldsymbol{E}$. This is the so–called magic γ. However, the muons are rather unstable and decay spontaneously after some time. When running at the magic energy the muons are highly relativistic, they travel almost at the speed of light with energies of about $E_{\text{magic}} = \gamma m_\mu c^2 \approx 3.098\ GeV$. Luckily, $\gamma = \sqrt{1 + 1/a_\mu} \approx 29.3$ is large enough to provide the time dilatation factor for the unstable muons boosting the lifetime of a muon at rest $\tau_\mu = 2.19711\ \mu s$ to its lifetime in the ring $\tau_{\text{flight}} = 64.435\ \mu s$. Thus, with their lifetime being much larger than at rest, muons are circling in the ring many times before they decay into a positron plus two neutrinos: $\mu^+ \to e^+ + \nu_e + \bar{\nu}_\mu$.

At the end we are left with

$$\omega_{\text{a}} = \frac{e}{m_\mu} a_\mu \mathbf{B} \tag{1.13}$$

which means that to measure a_μ, we must precisely measure ω_a and $\boldsymbol{B}$. The muon mass m_μ is obtained from an independent experiment on muonium (for a more detailed description see [40, 53] and references therein).

1.2.1 Fermilab E989 experiment

The E989 experiment begins with protons. About 12 times per second, Fermilab's accelerators smash a bunch of protons into a fixed target, creating different types of particles. Scientists are interested in the emerging pions, which quickly decay into muons with aligned spins. Magnets steer the pions and the resulting muons into a triangular-shaped tunnel called the Muon Delivery Ring. As the particles travel hundreds of meters around the ring, essentially all of the pions decay into muons

$$\pi^+ \to \mu^+ + \nu_\mu, \quad \pi^- \to \mu^- + \overline{\nu}_\mu \tag{1.14}$$

This beam of muons is then transferred into the experiment's precision storage ring, which was used in the Brookhaven E821 experiment.

As the muons travel around the ring, they are decaying into neutrinos and positrons

$$\mu^+ \to e^+ + \nu_e + \overline{\nu}_\mu, \quad \mu^- \to e^- + \overline{\nu}_e + \nu_\mu \tag{1.15}$$

The neutrinos fly away undetected, but the positrons, which travel in the same direction that the muon's spin was pointing, can be measured. The ω_a measurement is performed by detecting them and fitting the time distribution of the decays with a five-parameter fit. The magnitude of the magnetic field in the storage ring will be 1.45 T and must be as constant as possible [40].

1.2.2 Muon $g-2$ experimental results

A summary of the anomalous magnetic moment a_μ results from the various experiments and data sets, showing the evolution of the experimental precision over time is shown in Fig. 1.3.

Experiment	Year	Polarity	$a_\mu \times 10^{10}$	Precision [ppm]
CERN I	1961	μ^+	11 450 000 (220000)	4300
CERN II	1962–1968	μ^+	11 661 600 (3100)	270
CERN III	1974–1976	μ^+	11 659 100 (110)	10
CERN III	1975–1976	μ^-	11 659 360 (120)	10
BNL	1997	μ^+	11 659 251 (150)	13
BNL	1998	μ^+	11 659 191 (59)	5
BNL	1999	μ^+	11 659 202 (15)	1.3
BNL	2000	μ^+	11 659 204 (9)	0.73
BNL	2001	μ^-	11 659 214 (9)	0.72
	Average		11 659 208.0 (6.3)	0.54

FIGURE 1.3: Summary of CERN and E821 results. Adapted from [40].

To underscore the tremendous improvement over time in experimental precision, the most recent measurements are presented graphically in Fig. 1.4.

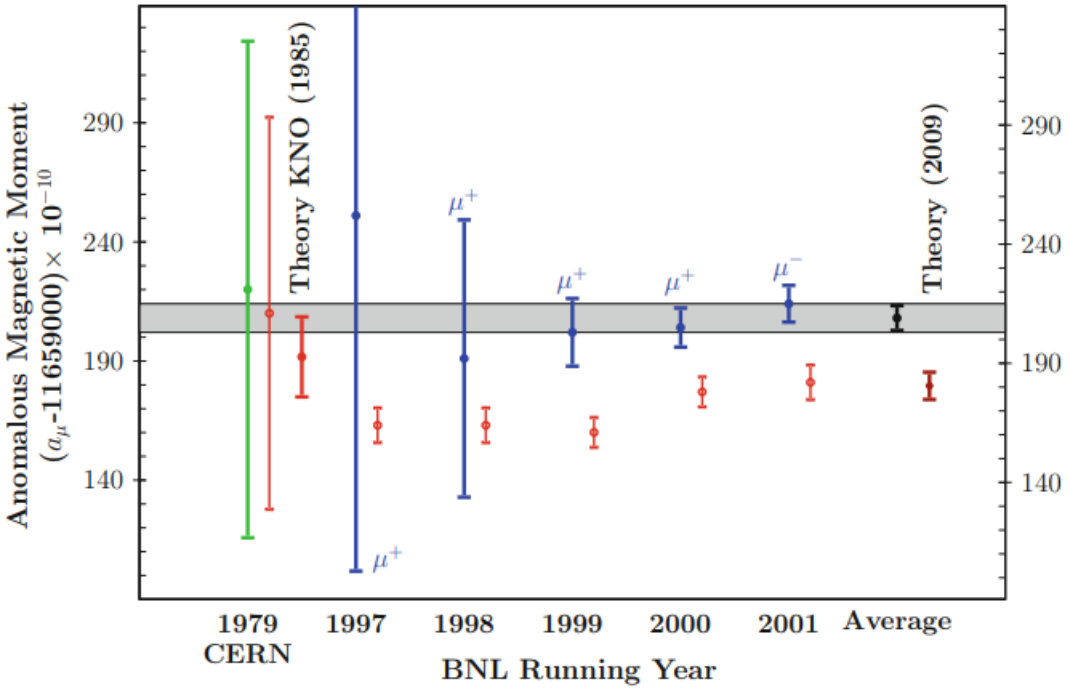

FIGURE 1.4: Results for the individual E821 measurements, together with the new world average and the theoretical prediction. The CERN result is shown together with the theoretical prediction by Kinoshita et al. 1985. The dotted vertical bars indicate the theory values quoted by the experiments. Adapted from [40].

The most updated experimental value for a_μ is given by

$$a_\mu^{\text{exp}} = 11659209.1(5.4)(3.3)[6.3] \times 10^{-10}, \tag{1.16}$$

as an average of

$$a_{\mu^-} = 11659215(8)(3) \times 10^{10} \quad \text{and} \tag{1.17}$$

$$a_{\mu^+} = 11659204(6)(5) \times 10^{10}. \tag{1.18}$$

The first uncertainty is statistical and the second systematic. The total error is given where statistical and systematic errors have been added in quadrature and it is represented by a bracket [40, 50].

1.3 Standard Model contributions to a_μ

In this section we give an overview of the different contributions to the anomalous magnetic moment of the muon a_μ considering the Standard Model of particle physics as a frame of reference. We show where the magnetic moment appears in the Standard Model, and we discuss the QED, QCD and weak interaction contributions. Finally, we compare the extracted values from experiment and theory.

As we have seen in Sect. 1.1, in the absence of electrical fields $\boldsymbol{E}$ the quantum correction of the magnetic moment of a lepton can be represented with a single number, the anomalous magnetic moment, which is the result of radiative corrections (RC). Since we are considering the interaction of a particle in an external magnetic field, in order to study the radiative corrections we have to extend the discussion of the preceding section and consider the full QED interaction Lagrangian

$$\mathcal{L}_{\text{int}}^{\text{QED}} = -e\overline{\psi}\gamma^\mu\psi A_\mu \tag{1.19}$$

where the photon field is a part of the dynamics but has an external classical component A_μ^{ext}

$$A_\mu \to A_\mu + A_\mu^{\text{ext}}. \tag{1.20}$$

Therefore we have to add to our set of contributions to the matrix element for the scattering amplitude, an additional external field vertex $-ie\gamma^\mu A_\mu^{\text{ext}}$ [40]

As we have seen, the magnetic moment is related to the interaction of spin particles with an external electromagnetic field. Then, in order to identify a_μ we simply have to take into account Feynman diagrams where a photon is interacting with a fermion (in our case a muon) (see Fig. 1.5).

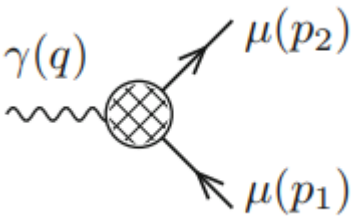

FIGURE 1.5: General Feynman diagram used to derive the contributions to the muon anomalous magnetic moment. q is the photon's four momenta, while p_1 and p_2 are muon's four-momenta. The shaded circle indicates the sum of the lowest-order muon-photon vertex and all amputated loop corrections. Reproduced from [40].

We can identify this diagram with the following expression

$$(-ie)\overline{u}\left(p_2\right)\Gamma^\mu u\left(p_1\right) = (-ie)\overline{u}\left(p_2\right)\left[\gamma^\mu F_{\text{E}}\left(q^2\right) + i\frac{\sigma^{\mu\nu}q_\nu}{2m_\mu}F_{\text{M}}\left(q^2\right)\right]u\left(p_1\right) \tag{1.21}$$

where Γ^μ is the muon-photon vertex function, $u(p)$ denote the Dirac spinors, $q = p_2 - p_1$, $F_E(q^2)$ is the electric charge or Dirac form factor and $F_M(q^2)$ is the magnetic or Pauli form factor. Note that the matrix $\sigma^{\mu\nu} = \frac{\mathrm{i}}{2}\left[\gamma^\mu, \gamma^\nu\right]$ represents the spin 1/2

angular momentum tensor. Taking into account the static limit, where there is no momentum transfer $q^2 = (p_2 - p_1)^2 \to 0$, we have

$$F_{\mathrm{E}}(0) = 1, \quad F_{\mathrm{M}}(0) = a_\mu \tag{1.22}$$

where the first equation is the charge renormalization condition (in units of the physical positron charge e), and the second one is the prediction for a_μ, in terms of the form factor F_M [40].

The small correction a_μ is consequence of many contributions which will be discussed in the following.

1.3.1 Quantum electrodynamics

By far the largest contribution to a_μ comes from interactions described by QED, which involve only diagrams containing leptons and photons. Contributions are calculated perturbatively as the expansion in powers of α/π. Each loop leads to a factor α/π [29].

Diagrams with virtual photons and muon loops

In this contribution only muons and photons are present, therefore it is mass independent.

- **1-loop diagram** [1 diagram]: It is the largest correction to the magnetic moment of the muon. It arises from the coupling to a single virtual photon as shown in Fig. 1.6. This one-loop diagram leads to the famous Schwinger result

$$a_\mu^{(2)} = \frac{\alpha}{2\pi} \tag{1.23}$$

- **2-loop diagrams** [7 diagrams]
- **3-loop diagrams** [72 diagrams]
- **4-loop diagrams** [891 diagrams]
- **5-loop diagrams** [12672 diagrams]

Diagrams with one, two and three loops have been evaluated analytically. Nevertheless, for a complete evaluation of four and five loop diagrams one has to use numerical methods. These two contributions are updating with time because of the progresses in computing technology (for a detailed discussion with results and figures see [40]).

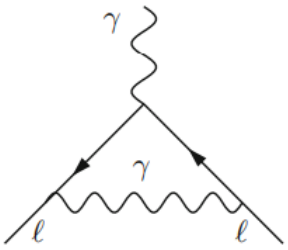

FIGURE 1.6: The lowest order QED contribution to a_ℓ. Reproduced from [40].

Mass dependent diagrams

These terms include also electrons (lighter than muon) and tauons (heavier than muons), thus they depend on masses, specifically on mass ratios m_e/m_μ and m_τ/m_μ. There are two types of diagrams:

- **QED photon vacuum polarisation (QED VP):** The lowest possible diagrams are 2-loop diagrams represented in Fig. 1.7 (a, b and c). The diagram (b), which has a muon loop, was already counted in the mass independent contribution. The higher the mass of a virtual lepton, the smaller the contribution to a_μ. Thus the diagram (a) yields the largest power correction of diagrams of this type (for a detailed discussion see [40, 53]).

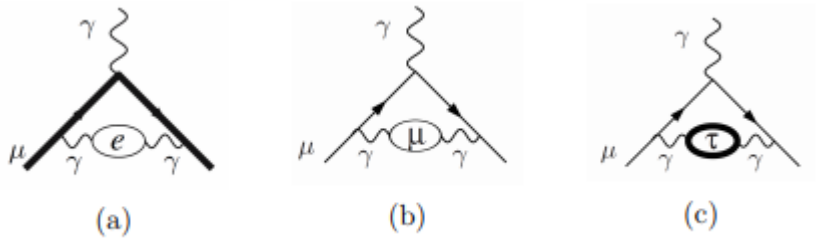

FIGURE 1.7: Three different 2-loop QED VP diagrams. Reproduced from [40].

- **QED Light-by-light scattering (QED LbL):** These diagrams are represented by closed fermion loops (in our case lepton) with four real photons attached ($\gamma\gamma \to \gamma\gamma$) (see Fig. 1.7 (a, b and c)). Remember that closed fermion loops with three photons vanish by Furry's theorem. The Feynman diagram (b) was actually considered in the first type of diagrams with virtual photons and muon loops. Again, this contribution depends on the mass of the internal lepton, hence the diagram that contributes the most is (a) [40, 53].

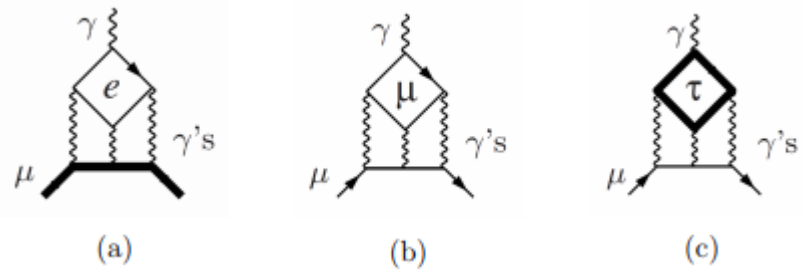

FIGURE 1.8: Representative QED light-by-light scattering diagrams. Reproduced from [40].

1.3.2 QCD

An important correction to a_μ is to include hadrons. Quantum chromodynamics (QCD) is the theory of strong interactions and shows up through the hadronic structure of the photon via vacuum polarisation starting at $O(\alpha^2)$ or light–by–light scattering starting at $O(\alpha^3)$. Formally, these are the contributions obtained by replacing lepton-loops by quark-loops (see Fig. 1.9). However quarks are strongly interacting via gluons as described by the $SU(3)_{\text{color}}$ gauge theory, and while electromagnetic and

weak interactions are weak in the sense that they allow us to perform perturbation expansions in the coupling constants, strong interactions are weak only at high energies. In the interesting regime, at energies below 2 GeV, the perturbative approach of QCD fails because the coupling constant increases (see Fig. 1.9). As before we divide the whole contribution into two parts:

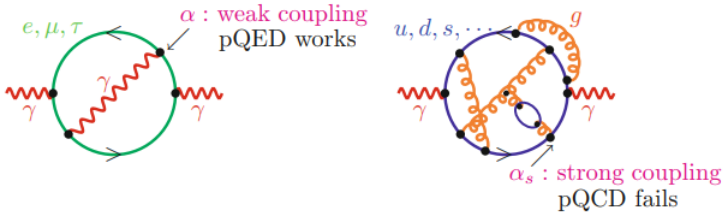

FIGURE 1.9: The hadronic analog of the lepton loops. One can see the main difference between QED and QCD: Because the coupling constant increases with decreasing energy, the quark-loop is full of quark-gluon plasma. This effect is the so-called anti-screening. Reproduced from [40].

Hadronic photon vacuum polarisation (HVP)

HVP processes, as illustrated in Fig. 1.10, provide the second-largest contribution to a_μ. Because QCD is non-perturbative at low energies, this term is difficult to calculate from first principles. Fortunately, it can be related to experimental data through the dispersion relation [29]. This correction can be evaluated by using causality (analyticity) and unitarity (optical theorem) together with experimental low energy data. The imaginary part of the photon self-energy Π_γ is calculated with the help of the optical theorem using the total cross-section of hadron production in electron-positron annihilation. Then, when we evaluate the diagram as a dispersion integral containing Π_γ, we get the a_μ contribution (for a recent calculation see [14]). An additional way to do this, is to make use of experimental τ-decay data [40].

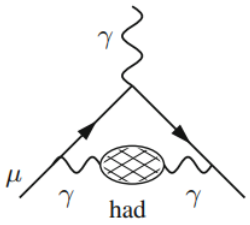

FIGURE 1.10: The leading order hadronic vacuum polarization diagram. Reproduced from [40].

Hadronic light-by-light scattering (HLbL)

HLbL scattering is a much more problematic set of hadronic corrections. Even for real-photon LbL scattering, perturbation theory is far from being able to describe reality, not to mention the non-perturbative approach [36, 41].

The HLbL scattering consists of a full four-point function made out of four-vector quark currents attached to the muon line with three of its legs coupling to photons in all possible ways and the fourth vector leg coupled to an on-shell external photon (see Fig. 1.11). The momenta flowing through the three vector legs of the four-point function attached to the muon line runs from zero up to infinity, then covering both

the non-perturbative and perturbative regimes of QCD. These two different regimes are separated by a scale of about 2 GeV. Above this scale, the strong interaction contributions have to match the perturbative QCD predictions in terms of quarks and gluons [9, 11].

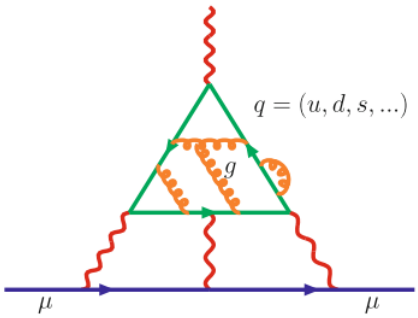

FIGURE 1.11: Hadronic light-by-light contribution to a_μ. Reproduced from [40].

The difficulty here is that, unlike the HVP, this contribution cannot be expressed in terms of experimental observables. In this case one has to resort to the low energy effective descriptions of QCD like Chiral Perturbation Theory (CHPT) extended to include vector-mesons. The so-called Resonance Lagrangian Approach (RLA), implements Vector Meson Dominance (VMD) in accord with chiral structure of QCD. Other effective theories are the Extended Nambu-Jona-Lasinio (ENJL) model or the very similar Hidden Local Symmetry (HLS) model [40]. Lattice QCD is also being used to provide estimates free from uncontrolled modelling assumptions. We will discuss the HLbL thoroughly in Chap. 2.

1.3.3 Weak interaction

Weak interaction, described by the electroweak (EW) Standard Model, is the last type of interaction that is contributing. Muon interacts weakly via heavy spin-one gauge boson ($W^\pm$ or Z) or via Higgs particle (H). The leading weak contributions in the unitary gauge are shown in Fig. 1.12. In spite of the fact that the unitary gauge is not renormalizable, the relevant gauge invariant S-matrix element, may be calculated directly in the unitary gauge. The advantage is that in this gauge only physical particles are present and diagrams exhibiting Higgs ghosts and Faddeev-Popov ghosts are absent. Notice that the diagram (a) exhibits a non-Abelian triple gauge vertex such that the corresponding contribution provides a test of the Yang-Mills structure involved [40].

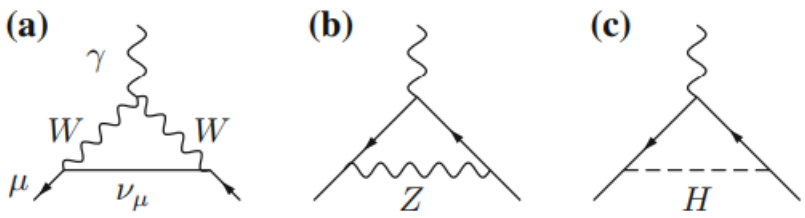

FIGURE 1.12: The leading weak contributions to a_μ; diagrams in the physical unitary gauge. Reproduced from [40].

The weak 2-loop corrections are also taken into account. They are the electromagnetic corrections of the 1-loop diagrams. Instead, the weak 3-loop effect remains uncalculated [40, 17]. Consequently, the electroweak error is dominated by the missing 3-loop contribution. However, the electroweak leading-log 3-loop effects of $\mathcal{O}\left[\frac{G_F}{\sqrt{2}}\frac{m_\mu^2}{8\pi^2}\left(\frac{\alpha}{\pi}\right)^2 \ln\frac{M_Z}{m_\mu}\right]$ has been evaluated using renormalization group arguments. The results show that those effects are negligible $\left[\sim \mathcal{O}\left(10^{-12}\right)\right]$ for the accuracy needed at present [53]. For a detailed calculation see e.g. [17].

1.3.4 Summary of Standard Model contributions

The common estimates for QED, QCD and EW corrections are collected in Fig. 1.13.

Contribution	Result in 10^{-10} units
QED (leptons)	11658471.885 ± 0.004
HVP (leading order)	690.8 ± 4.7
$\text{HVP}^{\text{NLO+NNLO}}$	-8.7 ± 0.1
HLBL	11.6 ± 4.0
EW	15.4 ± 0.1
Total	11659179.1 ± 6.2

FIGURE 1.13: Standard Model contributions to a_μ. Reproduced from [49]. For a detailed information see references therein.

1.4 Comparison between theory and experiment

As we have seen in equation (1.16), the most updated experimental value for a_μ is given by

$$a_\mu^{\text{exp}} = 11659209.1(5.4)(3.3)[6.3] \times 10^{-10}, \tag{1.24}$$

and the theoretical value obtained adding up all the contributions form the SM (see Fig. 1.13) is given by

$$a_\mu^{\text{SM}} = 11659179.1[6.2] \times 10^{-10}, \tag{1.25}$$

which gives an unexplained discrepancy

$$\Delta a_\mu = a_\mu^{\text{EXP}} - a_\mu^{\text{SM}} = (30.0 \pm 8.8) \times 10^{-10} \tag{1.26}$$

of about 3.4σ [49]. This difference is one of the main reasons why the anomalous magnetic moment is and will be in the next years, a very interesting field of study. It probes the borders of our understanding of particle properties in the Standard Model. If this difference cannot be resolved within the Standard Model, we need to look for new physics contributions not covered by QED, QCD and weak interaction. Some options for the reason of such difference are announced as follows:

- **Statistical uncertainties:** All the experiments of this type are statistical processes, so physicists could have measured large statistical fluctuation which is far away from the theoretical value.
- **Underestimated systematic errors:** Many different measurements are done to get the final result. Maybe all these contributions to systematic uncertainties are underestimated.

- **Incomprehension of the Standard Model:** The current SM (renormalizable electroweak theory and QCD) may not have been correctly evaluated. No one doubts in the main terms derived from QED and the weak interaction, but the calculation of the hadronic part of a_μ is complex and in some parts approximate. We actually do not know all the things that can contribute and that is the reason why the dispersive approach is used. Therefore, the biggest puzzle, in theory, is the hadronic part.

- **Physics beyond the Standard Model:** QED contributions have not an as important role for a_μ as for a_e. This is also the reason why a_μ is much more sensitive to BSM. There are contributions that cannot be explained with the SM, but we do not know what they actually are. See Sect. 1.4.1.

1.4.1 Possible contributions to a_μ from new physics

There are many interpretations of BSM that could handle with $a_\mu^{\text{EXP}} - a_\mu^{\text{SM}}$:

- Supersymmetry (SUSY)
- Dark photon
- Extra dimensions (ED)
- Additional Higgs bosons
- Radiative muon mass scenarios
- Anomalous W boson properties
- New gauge bosons
- Leptoquarks
- Bileptons

Nevertheless, our purpose here is not to intervene in this ongoing debate. For a detailed discussion see e.g. [40, 29].

Chapter 2

Framework

This chapter gives an overview of the method used as well as the calculations to extract the contributions to the anomalous magnetic moment of the muon from the hadronic light-by-light scattering (see Sect. 1.3.2 for an introduction of the HLbL).

The HLbL cannot be directly related to any measurable cross section and requires knowledge of QCD at all energy scales. Since this is not known yet, one needs to rely on hadronic models to compute it. Such models introduce systematic errors which are difficult to quantify. Using the large-N_c [67] and the chiral counting, de Rafael [7] proposed to split the HLbL into a set of different contributions: pseudo-scalar exchange (dominant), charged pion and kaon loops, quark loop, and higher-spin exchanges. The large-N_c approach however has at least two shortcomings: firstly, it is difficult to use experimental data in a large-N_c world. Secondly, calculations carried out in the large-N_c limit demand an infinite set of resonances [49]. Dealing with such sum remains cumbersome, and to a large extent illusory, since the characteristics of these states (masses, couplings, etc.) are in general not known. It has, however, been shown in several instances (see, e.g. [43] and references therein) that keeping, in each channel, only a finite number of resonances, supplemented with information on the QCD short-distance properties coming from the operator product expansion, already gives a good description of quantities like form factors or correlation functions in the Euclidean region, especially when they occur in weighted integrals over the whole range of momenta.

The structure of the chapter is as follows: We begin calculating the HLbL contribution to the anomalous magnetic moment of the muon a_μ. A complete discussion of the HLbL contribution involves the full rank-four hadronic vacuum polarization tensor $\Pi_{\mu\nu\lambda\rho}$, which is a rather involved object: Its general covariant decomposition involves 138 Lorentz structures. We focus on the pion-pole contribution. Fortunately, this contribution we are interested in corresponds to the lowest-mass part of $\Pi_{\mu\nu\lambda\rho}$ that is leading in the large-N_c limit, which might provide an explanation as to why it happens to constitute the dominant fraction of the light-by-light scattering correction to a_μ. We leave for future work a complete discussion of $\Pi_{\mu\nu\lambda\rho}$ within a theoretical framework close to the one adopted here (and discussed below) for the pion-pole contribution. We compute the pion-pole contribution to a_μ using the model from Knecht and Nyffeler [43]. The resulting two-loop integrals are treated by first performing the angular integration analytically, using the method of Gegenbauer polynomials, followed by a numerical evaluation of the remaining two-dimensional integration over the moduli of the Euclidean loop momenta. However, one needs a model for the transition form factor. Knecht and Nyffeler [43] considered form factors based on the large-N_c and short-distance properties of QCD, that involve either one vector resonance (lowest meson dominance, LMD) or two vector resonances (LMD + V). Instead, in our thesis, we extend the vector meson dominance (VMD) and LMD transition form factors by summing up the infinite number of zero-width resonances

that appear in the large-N_c limit. In order to do so, the masses and couplings of the zero-width states are fixed so that the form factors become Euler Beta functions of the Veneziano type, involving one single free parameter which controls their asymptotic power behaviour. This model is called Dual-Large N_c. Following this scheme, we also discuss the η and η' poles in order to give a total value for the pseudoscalar contribution, and the electromagnetic form factor of the pion used to compute the pion-loop.

2.1 Calculating the HLbL contribution

The hadronic light–by–light scattering contribution to the muon electromagnetic vertex function $\Gamma^{\mu}\left(p',p\right)$ is represented by the diagram Fig. 2.1. According to this diagram, the vertex matrix element is given by [40]

$$\begin{aligned}
&\left\langle \mu^{-}\left(p'\right)\left|(ie)j_{\rho}(0)\right|\mu^{-}(p)\right\rangle = (-ie)\ \overline{u}\left(p'\right)\Gamma_{\rho}\left(p',p\right)u(p)\\
&=\int\frac{\mathrm{d}^{4}q_{1}}{(2\pi)^{4}}\frac{\mathrm{d}^{4}q_{2}}{(2\pi)^{4}}\frac{(-\mathrm{i})^{3}}{q_{1}^{2}q_{2}^{2}\left(q_{1}+q_{2}-k\right)^{2}}\frac{\mathrm{i}}{\left(p'-q_{1}\right)^{2}-m^{2}}\frac{\mathrm{i}}{\left(p-q_{1}-q_{2}\right)^{2}-m^{2}}\\
&\times(-ie)^{3}\ \overline{u}\left(p'\right)\gamma^{\mu}\left(\not{p}'-\not{q}_{1}+m\right)\gamma^{\nu}\left(\not{p}-\not{q}_{1}-\not{q}_{2}+m\right)\gamma^{\lambda}\ u(p)\\
&\times(ie)^{4}\ \Pi_{\mu\nu\lambda\rho}\left(q_{1},q_{2},k-q_{1}-q_{2}\right)
\end{aligned}\tag{2.1}$$

where

$$\begin{aligned}
\Pi_{\mu\nu\lambda\rho}\left(q_{1},q_{2},q_{3}\right) = &\int\mathrm{d}^{4}x_{1}\ \mathrm{d}^{4}x_{2}\ \mathrm{d}^{4}x_{3}\ e^{i(q_{1}x_{1}+q_{2}x_{2}+q_{3}x_{3})}\\
&\times\left\langle 0\left|\ T\left\{j_{\mu}\left(x_{1}\right)j_{\nu}\left(x_{2}\right)j_{\lambda}\left(x_{3}\right)j_{\rho}(0)\right\}\ \right|0\right\rangle
\end{aligned}\tag{2.2}$$

is the full rank–four hadronic vacuum polarization tensor with $|\Omega\rangle$ denoting the QCD vacuum. The Momentum $k=p'-p$ of the external photon is incoming, while the q_i's of the virtual photons are outgoing from the hadronic "blob". Here $j_{\mu}(x)$ denotes the light quark part of the electromagnetic current

$$j_{\mu}(x)=\frac{2}{3}\left(\overline{u}\gamma_{\mu}u\right)(x)-\frac{1}{3}\left(\overline{d}\gamma_{\mu}d\right)(x)-\frac{1}{3}\left(\overline{s}\gamma_{\mu}s\right)(x)\equiv\overline{q}\hat{Q}\gamma_{\mu}q(x)\tag{2.3}$$

It includes a summation over color of the color and flavour diagonal quark bilinears.

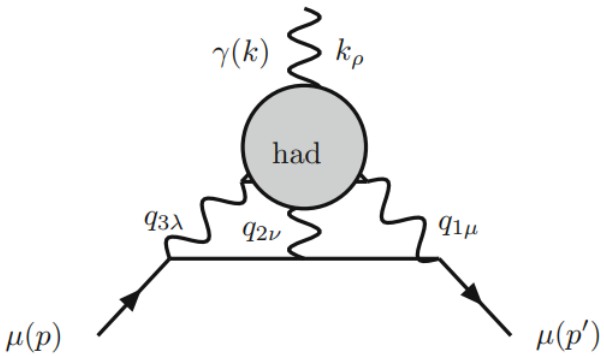

FIGURE 2.1: Setup for the calculation of the hadronic contribution of the light–by–light scattering to the muon electromagnetic vertex $\Gamma^{\mu}\left(p',p\right)$. Adapted from [40].

Since the electromagnetic current $j_\mu(x)$ is conserved, the tensor $\Pi_{\mu\nu\lambda\rho}(q_1,q_2,q_3)$ satisfies the Ward-Takahashi identities

$$\left\{q_1^\mu; q_2^\nu; q_3^\lambda; k^\rho\right\} \Pi_{\mu\nu\lambda\rho}\left(q_1,q_2,q_3\right) = 0 \tag{2.4}$$

with $k=(q_1+q_2+q_3)$. Taking the derivative $\frac{\partial}{\partial k^\rho}$ of $k^\rho \Pi_{\mu\nu\lambda\rho}(q_1,q_2,k-q_1-q_2)=0$ implies

$$\Pi_{\mu\nu\lambda\rho}\left(q_1,q_2,k-q_1-q_2\right) = -k^\sigma \left(\partial/\partial k^\rho\right) \Pi_{\mu\nu\lambda\sigma}\left(q_1,q_2,k-q_1-q_2\right). \tag{2.5}$$

Up to one-loop, the electromagnetic $\overline{\ell}\ell\gamma$-vertex was discussed in Sect. 1.3, where we deduced

$$\overline{u}\left(p'\right)\Gamma_\rho\left(p',p\right)\ u\left(p\right) = \overline{u}\left(p'\right)\left[\gamma_\rho\ F_{\mathrm{E}}\left(k^2\right) + i\frac{\sigma_{\rho\tau}k^\tau}{2m_\mu}F_{\mathrm{M}}\left(k^2\right)\right] u\left(p\right) \tag{2.6}$$

and

$$F_{\mathrm{E}}(0)=1, \quad F_{\mathrm{M}}(0)=a_\mu. \tag{2.7}$$

Now, using equation (2.5) we obtain $\Gamma_\rho\left(p',p\right) = k^\sigma \Gamma_{\rho\sigma}\left(p',p\right)$, which inserted in equation (2.1) with (2.5) gives

$$\begin{aligned}
&\overline{u}\left(p'\right)\Gamma_{\rho\sigma}\left(p',p\right)u(p) = -ie^6 \\
&\times \int \frac{\mathrm{d}^4q_1}{(2\pi)^4}\frac{\mathrm{d}^4q_2}{(2\pi)^4}\frac{1}{q_1^2q_2^2\left(q_1+q_2-k\right)^2}\frac{1}{\left(p'-q_1\right)^2-m^2}\frac{1}{\left(p-q_1-q_2\right)^2-m^2} \\
&\times \overline{u}\left(p'\right)\gamma^\mu\left(\not{p}'-\not{q}_1+m\right)\gamma^\nu\left(\not{p}-\not{q}_1-\not{q}_2+m\right)\gamma^\lambda\ u(p) \\
&\times \frac{\partial}{\partial k^\rho}\ \Pi_{\mu\nu\lambda\sigma}\left(q_1,q_2,k-q_1-q_2\right)
\end{aligned} \tag{2.8}$$

As stated in equation (2.7), we are interested in extracting the form factor F_{M}. One may project out the form factors directly from the vertex function $\Gamma_\rho\left(p',p\right)$ using a projection operator technique (see e.g. [40, 58]). Considering the Ward-Takahashi identities $k^\rho k^\sigma\ \overline{u}\left(p'\right)\Gamma_{\rho\sigma}\left(p',p\right)u(p)=0$ and this technique, one obtains

$$F_M\left(k^2\right) = \mathrm{Tr}\left\{\left(\not{p}+m\right)\Lambda_\rho^{(2)}\left(p',p\right)\left(\not{p}'+m\right)\Gamma^\rho\left(p',p\right)\right\} \tag{2.9}$$

with the help of the projector

$$\Lambda_\rho^{(2)}\left(p',p\right) = \frac{m^2}{k^2\left(4m^2-k^2\right)}\left[\gamma_\rho + \frac{k^2+2m^2}{m\left(k^2-4m^2\right)}\left(p'+p\right)_\rho\right]. \tag{2.10}$$

In order to obtain the muon anomaly we need to work out the classical limit of the form factor $F_M\left(k^2\right)$

$$a_\mu = \lim_{k^2\to 0} F_2\left(k^2\right) \tag{2.11}$$

such that

$$F_{\mathrm{M}}(0) = \frac{1}{48m}\,\mathrm{Tr}\left\{\left(\not{p}+m\right)\left[\gamma^\rho,\gamma^\sigma\right]\left(\not{p}+m\right)\Gamma_{\rho\sigma}(p,p)\right\} \tag{2.12}$$

and finally

$$
\begin{aligned}
a_\mu = & \frac{-ie^6}{48m} \int \frac{\mathrm{d}^4q_1}{(2\pi)^4} \frac{\mathrm{d}^4q_2}{(2\pi)^4} \frac{1}{q_1^2 q_2^2 \left(q_1+q_2\right)^2} \frac{1}{\left(p-q_1\right)^2 - m^2} \frac{1}{\left(p-q_1-q_2\right)^2 - m^2} \\
& \times \mathrm{Tr}\left\{ \left(\not{p}+m\right) \left[\gamma^\rho, \gamma^\sigma\right] \left(\not{p}+m\right) \gamma^\mu \left(\not{p}-\not{q}_1+m\right) \gamma^\nu \left(\not{p}-\not{q}_1-\not{q}_2+m\right) \gamma^\lambda \right\} \\
& \times \left(\frac{\partial}{\partial k^\rho} \Pi_{\mu\nu\lambda\sigma}\left(q_1, q_2, k-q_1-q_2\right) \right)_{k=0} .
\end{aligned}
\tag{2.13}
$$

This is what we actually need to calculate. The integral to be performed is 8 dimensional, where 3 integrations can be done analytically. In general, one has to deal with a 5 dimensional non-trivial integration over 3 angles and 2 moduli.

2.1.1 Full rank-four hadronic vacuum polarization tensor $\Pi_{\mu\nu\lambda\rho}$

The hadronic tensor $\Pi_{\mu\nu\lambda\sigma}\left(q_1, q_2, k-q_1-q_2\right)$ we have to deal with, is a problematic object, because it has an unexpectedly complex structure as we will see, in no way comparable with the leptonic counterpart. The general covariant decomposition involves 138 Lorentz structures [40]:

$$
\begin{aligned}
\Pi^{\mu\nu\alpha\beta}\left(p_1,p_2,p_3\right) \equiv & \Pi^1\left(p_1,p_2,p_3\right) g^{\mu\nu}g^{\alpha\beta} + \Pi^2\left(p_1,p_2,p_3\right) g^{\mu\alpha}g^{\nu\beta} \\
& + \Pi^3\left(p_1,p_2,p_3\right) g^{\mu\beta}g^{\nu\alpha} \\
& + \Pi^{1jk}\left(p_1,p_2,p_3\right) g^{\mu\nu}p_j^\alpha p_k^\beta + \Pi^{2jk}\left(p_1,p_2,p_3\right) g^{\mu\alpha}p_j^\nu p_k^\beta \\
& + \Pi^{3jk}\left(p_1,p_2,p_3\right) g^{\mu\beta}p_j^\nu p_k^\alpha + \Pi^{4jk}\left(p_1,p_2,p_3\right) g^{\nu\alpha}p_j^\mu p_k^\beta \\
& + \Pi^{5jk}\left(p_1,p_2,p_3\right) g^{\nu\beta}p_j^\mu p_k^\alpha + \Pi^{6jk}\left(p_1,p_2,p_3\right) g^{\alpha\beta}p_j^\mu p_k^\nu \\
& + \Pi^{ijkm}\left(p_1,p_2,p_3\right) p_i^\mu p_j^\nu p_k^\beta p_m^\alpha
\end{aligned}
\tag{2.14}
$$

where $i,j,k,m = 1,2$ or 3 and repeated indices are summed. The functions are scalar functions of all possible invariant products $p_i \cdot p_j$. By the WT identities and the kinematical constraint $k_\mu \to 0$ the number of amplitudes contributing to $g-2$ reduces to 32. In fact as shown recently in [68], the number of amplitudes contributing to $g-2$ can be reduced to 19 independent ones if one takes into account the symmetry of the integral under permutations of the three virtual photons [40].

As mentioned at the beginning of this chapter already, using the large-N_c [67] and the chiral counting, de Rafael [7] proposed to split the HLbL into a set of different contributions: pseudo-scalar exchange (dominant), charged pion and kaon loops, quark loop, and higher-spin exchanges (see Fig. 2.2). Among these contributions, the pseudo-scalar exchange, charged pion and kaon loops, and higher-spin exchanges dominate at long distances (L.D.) and the quark loops including hard gluonic corrections dominate at short distances (S.D.). Generally, the perturbative QCD expansion only is useful to evaluate the short distance tail, while the dominant long distance part must be evaluated using some low energy effective mode which includes the vector mesons (the photons in the effective theory couple to hadrons via $\gamma - \rho^0$ mixing).

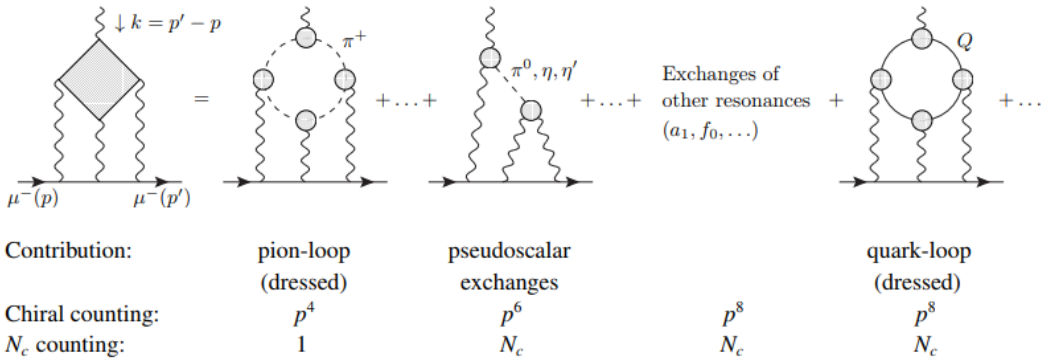

FIGURE 2.2: The different contributions to HLbL scattering in the muon $g-2$ and their leading order in the chiral expansion p^2 and their large-N_c counting. Adapted from [57].

For the models presented so far one is confronted with the problem that one has to complement a non-renormalizable effective theory with renormalizable perturbative QCD above a certain cut-off. This generally results in a substantial cut-off dependence of the results. In order to avoid this matching problem, the most recent estimations attempt to resort to quark-hadron duality for matching L.D. and S.D. physics. This duality can be proven to hold in the large-Nc limit of QCD and this may be exploited in an $1/N_c$ expansion approach to QCD. However, once more the $N_c \to \infty$ limit, in which the hadrons turn out to be an infinite series of vector resonances, is not under quantitative control. Hence, a further approximation must be made by replacing the infinite series of narrow resonances by a few low lying states which are identified with existing hadronic states. As a result one obtains a modeling of the hadronic amplitudes, the simplest one being the lowest meson dominance (LMD) or minimal hadronic ansatz (MHA) approximation to large-Nc QCD [40].

2.2 Pion-pole contribution

The contribution form the light pseudoscalars π^0, η and η' is numerically dominant according to most model calculations [57, 49]. Because of this observation, there are many evaluations of this contribution following different approaches (see e.g. [50, 57, 56] and [49] for a review of the most updated approaches).

Here, we concentrate on the contributions to $\Pi_{\mu\nu\lambda\rho}(q_1, q_2, q_3)$ arising from single neutral pion exchanges. The corresponding diagrams (see Fig. 2.3) read as follows [43]

$$\begin{aligned}
&\Pi^{(\pi^0)}_{\mu\nu\lambda\rho}(q_1, q_2, q_3) \\
&= i\frac{\mathcal{F}_{\pi^0\gamma^*\gamma^*}(q_1^2, q_2^2)\mathcal{F}_{\pi^0\gamma^*\gamma^*}(q_3^2, (q_1+q_2+q_3)^2)}{(q_1+q_2)^2 - M_\pi^2}\varepsilon_{\mu\nu\alpha\beta}q_1^\alpha q_2^\beta \varepsilon_{\lambda\rho\sigma\tau}q_3^\sigma (q_1+q_2)^\tau \\
&+ i\frac{\mathcal{F}_{\pi^0\gamma^*\gamma^*}(q_1^2, (q_1+q_2+q_3)^2)\mathcal{F}_{\pi^0\gamma^*\gamma^*}(q_2^2, q_3^2)}{(q_2+q_3)^2 - M_\pi^2}\varepsilon_{\mu\rho\alpha\beta}q_1^\alpha (q_2+q_3)^\beta \varepsilon_{\nu\lambda\sigma\tau}q_2^\sigma q_3^\tau \\
&+ i\frac{\mathcal{F}_{\pi^0\gamma^*\gamma^*}(q_1^2, q_3^2)\mathcal{F}_{\pi^0\gamma^*\gamma^*}(q_2^2, (q_1+q_2+q_3)^2)}{(q_1+q_3)^2 - M_\pi^2}\varepsilon_{\mu\lambda\alpha\beta}q_1^\alpha q_3^\beta \varepsilon_{\nu\rho\sigma\tau}q_2^\sigma (q_1+q_3)^\tau .
\end{aligned} \tag{2.15}$$

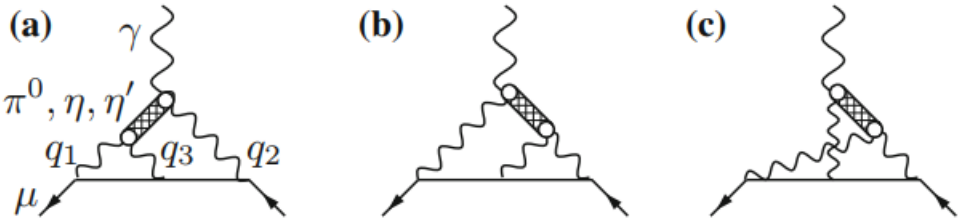

FIGURE 2.3: Pion-pole contributions to the HLbL scattering. Internal photons lines are dressed by $\rho-\gamma$ mixing. The blobs represent the form factor $\mathcal{F}_{\pi^0\gamma^*\gamma^*}$. Adapted from [40].

The key object here is the $\pi^0\gamma\gamma$ transition form factor $\mathcal{F}_{\pi^0\gamma^*\gamma^*}(m_\pi^2, q_1^2, q_2^2)$ which is defined by the matrix element

$$i\int d^4x e^{iq\cdot x}\left\langle \Omega\left|T\left\{j_\mu(x)j_\nu(0)\right\}\right|\pi^0(p)\right\rangle = \varepsilon_{\mu\nu\alpha\beta}q^\alpha p^\beta \mathcal{F}_{\pi^0\gamma^*\gamma^*}(m_\pi^2, q^2, (p-q)^2), \quad (2.16)$$

and it is Bose symmetric $\mathcal{F}_{\pi^{0*}\gamma^*\gamma^*}\left(s, q_1^2, q_2^2\right) = \mathcal{F}_{\pi^{0*}\gamma^*\gamma^*}\left(s, q_2^2, q_1^2\right)$, as the two photons are indistinguishable. An important point we should notice is that in the Feynman integral corresponding to one of the diagrams of Fig. 2.3, the pion is not necessarily near the pole, i.e. it holds for off-shell pions as well [40]. However, a seemingly plausible approximation which helps to simplify the calculation is to assume pion-pole dominance in the sense that one takes the form factor on the pion mass shell and uses $\mathcal{F}_{\pi^0\gamma^*\gamma^*}(m_\pi^2, q_1^2, q_2^2)$ everywhere. For now on, we are going to restrict our analysis to this approximation since we are interested in following the scheme of Knecht and Nyffeler [43], which uses this approximation. For the general pion-exchange case, see e.g. [40].

In order to compute a_μ we use equation (2.13) with the pion-pole contribution of the tensor $\Pi^{(\pi^0)}_{\mu\nu\lambda\rho}(q_1, q_2, q_3)$ (see equation (2.15)). Hence, we need

$$\begin{aligned}
&\frac{\partial}{\partial k^\rho}\Pi^{(\pi^0)}_{\mu\nu\lambda\sigma}(q_1, q_2, k-q_1-q_2)\\
&= i\frac{\mathcal{F}_{\pi^0\gamma^*\gamma^*}(q_1^2, q_2^2)\mathcal{F}_{\pi^0\gamma^*\gamma^*}((q_1+q_2)^2, 0)}{(q_1+q_2)^2 - M_\pi^2}\varepsilon_{\mu\nu\alpha\beta}q_1^\alpha q_2^\beta \varepsilon_{\lambda\sigma\rho\tau}(q_1+q_2)^\tau\\
&+ i\frac{\mathcal{F}_{\pi^0\gamma^*\gamma^*}(q_1^2, 0)\mathcal{F}_{\pi^0\gamma^*\gamma^*}(q_2^2, (q_1+q_2)^2)}{q_1^2 - M_\pi^2}\varepsilon_{\mu\sigma\tau\rho}q_1^\tau \varepsilon_{\nu\lambda\alpha\beta}q_1^\alpha q_2^\beta\\
&+ i\frac{\mathcal{F}_{\pi^0\gamma^*\gamma^*}(q_1^2, (q_1+q_2)^2)\mathcal{F}_{\pi^0\gamma^*\gamma^*}(q_2^2, 0)}{q_2^2 - M_\pi^2}\varepsilon_{\mu\lambda\alpha\beta}q_1^\alpha q_2^\beta \varepsilon_{\nu\sigma\rho\tau}q_2^\tau + \mathcal{O}(k)
\end{aligned} \quad (2.17)$$

Inserting this last expression into equation (2.13) and computing the corresponding Dirac traces, one obtains

$$\begin{aligned}
a_\mu^{\mathrm{LbyL};\pi^0} = -e^6 \int \frac{d^4q_1}{(2\pi)^4}\int \frac{d^4q_1}{(2\pi)^4}\frac{1}{q_1^2 q_2^2 (q_1+q_2)^2[(p+q_1)^2 - m^2][(p-q_2)^2 - m^2]}\\
\times\left[\frac{\mathcal{F}_{\pi^0\gamma^*\gamma^*}(q_1^2, (q_1+q_2)^2)\mathcal{F}_{\pi^0\gamma^*\gamma^*}(q_2^2, 0)}{q_2^2 - M_\pi^2}T_1(q_1, q_2; p)\right.\\
\left.+\frac{\mathcal{F}_{\pi^0\gamma^*\gamma^*}(q_1^2, q_2^2)\mathcal{F}_{\pi^0\gamma^*\gamma^*}((q_1+q_2)^2, 0)}{(q_1+q_2)^2 - M_\pi^2}T_2(q_1, q_2; p)\right]
\end{aligned} \quad (2.18)$$

with

$$T_1(q_1,q_2;p) = \frac{16}{3}(p\cdot q_1)(p\cdot q_2)(q_1\cdot q_2) - \frac{16}{3}(p\cdot q_2)^2 q_1^2 - \frac{8}{3}(p\cdot q_1)(q_1\cdot q_2)q_2^2 + 8(p\cdot q_2)q_1^2q_2^2 - \frac{16}{3}(p\cdot q_2)(q_1\cdot q_2)^2 + \frac{16}{3}m^2q_1^2q_2^2 - \frac{16}{3}m^2(q_1\cdot q_2)^2 \tag{2.19}$$

$$T_2(q_1,q_2;p) = \frac{16}{3}(p\cdot q_1)(p\cdot q_2)(q_1\cdot q_2) - \frac{16}{3}(p\cdot q_1)^2 q_2^2 + \frac{8}{3}(p\cdot q_1)(q_1\cdot q_2)q_2^2 + \frac{8}{3}(p\cdot q_1)q_1^2q_2^2 + \frac{8}{3}m^2q_1^2q_2^2 - \frac{8}{3}m^2(q_1\cdot q_2)^2 \tag{2.20}$$

In deriving equation (2.18), we have used the fact that, upon a trivial change of variables in the two-loop integral of equation (2.13), the two first terms of equation (2.15) lead to identical contributions. That is, diagrams (a) and (b) from Fig. 2.3 give rise to identical contributions involving the function $T_1(q_1,q_2;p)$, whereas (c) gives the contribution involving $T_2(q_1,q_2;p)$. Furthermore, in writing $T_2(q_1,q_2;p)$ we have taken into account the invariance of the remaining factors of the corresponding integrand under the exchange $q_1 \leftrightarrow q_2$. At this stage everything is known besides the $\pi^0\gamma\gamma$ transition form factors.

2.2.1 $\pi^0\gamma\gamma$ transition form factor

Above we have formally reduced the problem of calculating the pion-pole contribution from the diagrams of Fig. 2.3 to the problem of calculating the integral (2.18). The non-perturbative aspect is now confined in the form factor $\mathcal{F}_{\pi^0\gamma^*\gamma^*}(m_\pi^2,q_1^2,q_2^2)$, which is not known as well as it would be desirable. For the time being we have to use hadronic models together with pQCD as a constraint on the high energy asymptotic behavior. Fortunately some experimental data are also available. The constant $\mathcal{F}_{\pi^0\gamma\gamma}(m_\pi^2,0,0)$ is well determined as [40]

$$\mathcal{F}_{\pi^0\gamma\gamma}(m_\pi^2,0,0) = \frac{1}{4\pi^2 F_\pi} \tag{2.21}$$

by the $\pi^0 \to \gamma\gamma$ decay rate, where $F_\pi \approx 92.4\ MeV$ is the pion decay constant [5, 8]. Notice that in many theoretical papers our F_π is denoted as $F_\pi\sqrt{2} \approx 130\ MeV$.

Additional experimental information is available for $\mathcal{F}_{\pi^0\gamma^*\gamma}(m_\pi^2,-Q^2,0)$ coming from experiments $e^+e^- \to e^+e^-\pi^0$ (see Fig. 2.4) where the electron (positron) gets tagged, i.e. selected according to appropriate kinematic criteria, such that $Q^2 = -(p_b-p_t)^2 = 2E_bE_t(1-\cos\Theta_t)$ is large. p_b is the beam electron (positron) four-momentum, p_t the one of the tagged electron (positron) and Θ_t is the angle between p_t and p_b. The differential cross section is then strongly peaked towards zero momentum transfer of the untagged positron (electron) which allows experiments to extract the form factor [40]. The experimental data on $\mathcal{F}_{\pi^0\gamma^*\gamma}(m_\pi^2,-Q^2,0)$ is available from CELLO [6] and CLEO [31], and from the recently new experiments from BaBar [3] and Belle [71]. This information reduces the model dependence.

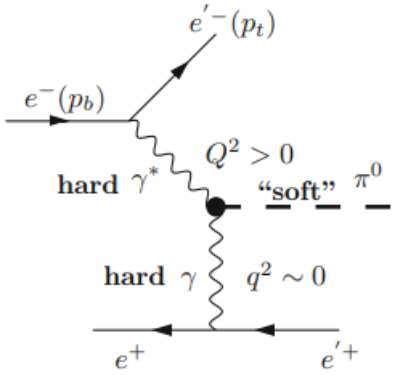

FIGURE 2.4: Measurement of the π^0 form factor $\mathcal{F}_{\pi^0\gamma^*\gamma}(m_\pi^2, -Q^2, 0)$ at high space-like Q_2 momentum. Adapted from [40].

Nevertheless, no sufficiently complete experimental information on the double off-shell $\pi^0\gamma\gamma$ transition form factor $\mathcal{F}_{\pi^0\gamma^*\gamma^*}(m_\pi^2, q_1^2, q_2^2)$ is available at the time being [43]. Resort to theory is therefore unavoidable. From the QCD perspective, the theoretical knowledge of $\mathcal{F}_{\pi^0\gamma^*\gamma^*}$ is sparse. However, there exists a well-defined limit of QCD where the situation improves somewhat, namely, the limit of infinite number of colors N_c. As N_c becomes large, the spectrum of QCD reduces, in each channel with given quantum numbers, to an infinite tower of zero-width resonances. As a consequence, the analytic structure of the form factor $\mathcal{F}_{\pi^0\gamma^*\gamma^*}(m_\pi^2, q_1^2, q_2^2)$ becomes simpler: it consists of a succession of simple poles, due to the contributions of zero-width $J^{PC} = 1--$ states (e.g. the ρ meson and its radial excitations) in each channel,

$$\mathcal{F}_{\pi^0\gamma^*\gamma^*}\,(q_1^2, q_2^2)\big|_{N_C\to\infty} = \sum_{ij} \frac{c_{ij}(q_1^2, q_2^2)}{(q_1^2 - M_{V_i}^2)(q_2^2 - M_{V_j}^2)} \tag{2.22}$$

where the sum runs over the infinite tower of zero-width vector resonances of large-N_c QCD. As mentioned at the beginning of this chapter, dealing with such sum remains cumbersome, since the characteristics of these states (masses, couplings, etc.) are in general not known. However keeping in each channel only a finite number of resonance, supplemented with information on the QCD short-distance properties coming from the operator product expansion, already gives a good description of quantities like form factors or correlation functions in the Euclidean region, especially when they occur in weighted integrals over the whole range of momenta.

In our thesis, we truncate the infinite sum to one vector resonance per channel, such that we obtain the vector meson dominance (VMD) and the lowest meson dominance (LMD) form factors [43]

$$\mathcal{F}^{VMD}_{\pi^0\gamma^*\gamma^*}\left(q_1^2, q_2^2\right) = -\frac{N_C}{12\pi^2 F_\pi} \frac{M_V^2}{\left(q_1^2 - M_V^2\right)} \frac{M_V^2}{\left(q_2^2 - M_V^2\right)} \tag{2.23}$$

$$\mathcal{F}^{LMD}_{\pi^0\gamma^*\gamma^*}\left(q_1^2, q_2^2\right) = \frac{F_\pi}{3} \frac{q_1^2 + q_2^2 - \frac{N_C}{4\pi^2}\frac{M_V^4}{F_\pi^2}}{\left(q_1^2 - M_V^2\right)\left(q_2^2 - M_V^2\right)} \tag{2.24}$$

That is, we perform the calculations with form factors of one vector resonance and in Sect. 2.4 we will extend these form factors in order to include the infinite sum of resonances. The reason is as follows: One observes that in equation (2.18) there are five independent variables $p \cdot q_1$, $p \cdot q_2$, q_1^2, q_2^2 and $q_1 \cdot q_2$, where $p \cdot q_i$ only occurs

in the fermion propagators, not in the form factors. It might therefore be possible to perform these two integrations analytically over $p \cdot q_1$ and $p \cdot q_2$ for general form factors. We would then be left with a three-dimensional integral, since the form factors depend on $q_1 \cdot q_2$. However, a crucial observation is that all dependences on $q_1 \cdot q_2$ in the numerators of $\mathcal{F}^{VMD}_{\pi^0\gamma^*\gamma^*}$ and $\mathcal{F}^{LMD}_{\pi^0\gamma^*\gamma^*}$ can be canceled by the ones in the resonance propagators. Therefore, we can write [43]

$$\mathcal{F}_{\pi^0\gamma^*\gamma^*}\left(q_1^2, q_2^2\right) = \frac{F_\pi}{3}\left[f\left(q_1^2\right) - \sum_{M_{V_i}} \frac{1}{q_2^2 - M_{V_i}^2} g_{M_{V_i}}\left(q_1^2\right)\right] \tag{2.25}$$

This representation, which seems to hold quite generally in the large-N_c limit of QCD, also extends to the Wess-Zumino-Witten (WZW) and the LMD+V (two vector resonances) form factors (for calculations with these two form factors, see [43]). The corresponding functions $f(q^2)$ and $g_{M_{V_i}}(q^2)$ can easily be worked out from the explicit expressions of the form factors (2.23) and (2.24). They are displayed in Fig. 2.5. For the VMD and LMD form factors, the sum in equation 2.25 reduces to a single term, and we call the corresponding function $g_{M_V}(q^2)$. Therefore, for the form factors that have the general form given by equation (2.25), it is possible to perform all angular integrations in the two-loop integral of equation (2.18) analytically. The extension of the VMD and LMD form factors can be performed afterwards by modifying the VMD and LMD propagators as we will see in Sect. 2.4.

	$f(q^2)$	$g_{M_V}(q^2)$
VMD	0	$\frac{N_C}{4\pi^2 F_\pi^2}\frac{M_V^4}{q^2 - M_V^2}$
LMD	$\frac{1}{q^2 - M_V^2}$	$-\frac{q^2 + M_V^2 - \frac{N_C}{4\pi^2}\frac{M_V^4}{F_\pi^2}}{q^2 - M_V^2}$

FIGURE 2.5: The functions $f(q^2)$ and $g_{M_V}(q^2)$ for the VMD and LMD form factors. Adapted from [43].

Taking into account equation (2.25) and using partial fractions, we can write the product of form factors in the two contributions of equation (2.18) as follows:

$$\begin{aligned}&\frac{\mathcal{F}_{\pi^0\gamma^*\gamma^*}(q_1^2, (q_1+q_2)^2)\mathcal{F}_{\pi^0\gamma^*\gamma^*}(q_2^2, 0)}{q_2^2 - M_\pi^2} \\ &= \frac{F_\pi}{3}\frac{\mathcal{F}_{\pi^0\gamma^*\gamma^*}\left(q_2^2, 0\right)}{q_2^2 - M_\pi^2}\left(f\left(q_1^2\right) - \frac{g_{M_V}\left(q_1^2\right)}{(q_1+q_2)^2 - M_V^2}\right)\end{aligned} \tag{2.26}$$

and

$$\begin{aligned}&\frac{\mathcal{F}_{\pi^0\gamma^*\gamma^*}(q_1^2, q_2^2)\mathcal{F}_{\pi^0\gamma^*\gamma^*}((q_1+q_2)^2, 0)}{(q_1+q_2)^2 - M_\pi^2} = \frac{F_\pi}{3}\mathcal{F}_{\pi^0\gamma^*\gamma^*}(q_1^2, q_2^2)\left(\frac{1}{(q_1+q_2)^2 - M_\pi^2}\right. \\ &\left.\times\left[f(0) + \frac{g_{M_V}(0)}{(M_V^2 - M_\pi^2)}\right] + \frac{g_{M_V}(0)}{\left[(q_1+q_2)^2 - M_V^2\right](M_\pi^2 - M_V^2)}\right)\end{aligned} \tag{2.27}$$

2.2.2 Gegenbauer polynomials (hyperspherical approach)

As we shall show in this section, for form factors that have the general form given by equation (2.25), it is possible to perform all angular integrations in the two-loop integral of equation (2.18) using the technique of Gegenbauer polynomials (hyperspherical approach). In order to do so, we perform a Wick rotation of the momenta q_1^μ, q_2^μ and p^μ, denoting by capital letters the rotated Euclidean momenta, with $Q_i^2 = -q_i^2$, $P^2 = -m^2$, etc.

The discussion of the angular integrals that can be found in the two-loop integral as well as the method of Gegenbauer polynomials used to solve them is presented in the work of Knecht and Nyffeler [43]. Since we go through the same calculations, we are not going to reproduce them again.

After having performed the angular integrations, the pion-pole contribution to $g-2$ can be written in a two-dimensional integral representation as follows [43]

$$a_\mu^{\mathrm{LbL};\pi^0} = \left(\frac{\alpha}{\pi}\right)^3 \left[a_\mu^{\mathrm{LbyL};\pi^0(1)} + a_\mu^{\mathrm{LbyL};\pi^0(2)}\right], \tag{2.28}$$

where

$$\begin{aligned} a_\mu^{\mathrm{LbL};\pi^0(1)} = &\int_0^\infty dQ_1 \int_0^\infty dQ_2 \Big[w_{f_1}(Q_1,Q_2)\, f^{(1)}\left(Q_1^2,Q_2^2\right) \\ &+ w_{g_1}(M_V,Q_1,Q_2)\, g_{M_V}^{(1)}\left(Q_1^2,Q_2^2\right) \Big] \end{aligned} \tag{2.29}$$

$$\begin{aligned} a_\mu^{\mathrm{LbL};\pi^0(2)} = &\int_0^\infty dQ_1 \int_0^\infty dQ_2 \\ &\times \sum_{M=M_\pi,M_V} w_{g_2}(M,Q_1,Q_2)\, g_M^{(2)}\left(Q_1^2,Q_2^2\right) \end{aligned} \tag{2.30}$$

with

$$f^{(1)}\left(Q_1^2,Q_2^2\right) = \frac{F_\pi}{3} f\left(-Q_1^2\right) \mathcal{F}_{\pi^0\gamma^*\gamma^*}\left(-Q_2^2,0\right) \tag{2.31}$$

$$g_{M_V}^{(1)}\left(Q_1^2,Q_2^2\right) = \frac{F_\pi}{3} \frac{g_{M_V}\left(-Q_1^2\right)}{M_V^2} \mathcal{F}_{\pi^0\gamma^*\gamma^*}\left(-Q_2^2,0\right) \tag{2.32}$$

$$g_{M_V}^{(2)}\left(Q_1^2,Q_2^2\right) = \frac{F_\pi}{3} \mathcal{F}_{\pi^0\gamma^*\gamma^*}\left(-Q_1^2,-Q_2^2\right) \frac{g_{M_V}(0)}{M_\pi^2 - M_V^2} \tag{2.33}$$

$$g_{M_\pi}^{(2)}\left(Q_1^2,Q_2^2\right) = \frac{F_\pi}{3} \mathcal{F}_{\pi^0\gamma^*y^*}\left(-Q_1^2,-Q_2^2\right) \left(f(0) + \frac{g_{M_V}(0)}{M_V^2 - M_\pi^2}\right) \tag{2.34}$$

Notice (see Fig. 2.5) that for the VMD model we have the simplifications $f^{(1)}\left(Q_1^2,Q_2^2\right) \equiv 0$ and $g_{M_V}^{(2)}\left(Q_1^2,Q_2^2\right) = -g_{M_\pi}^{(2)}\left(Q_1^2,Q_2^2\right)$, since $f^{VMD}\left(-Q_1^2\right) \equiv 0$.

The universal (for the class of form factors that have a representation of the type (2.25)) weight functions w that appear in equations (2.29) and (2.30) are given by

$$
\begin{aligned}
w_{f_1}(Q_1,Q_2) = {} & \frac{\pi^2}{Q_2^2+M_\pi^2}\frac{1}{6m^2Q_1Q_2}\Bigg\{-4\left(2m^2-Q_2^2\right)\left(Q_1^2-Q_2^2\right)^2 \\
& \times\ln\left[1+\frac{\left(Q_1^2+Q_2^2-R^0\right)\left(Q_1^2-R_1^m\right)\left(Q_2^2-R_2^m\right)}{8m^2Q_1^2Q_2^2}\right] \\
& +\left[-4m^2Q_1^2Q_2^2-\frac{1}{m^2}Q_1^4Q_2^4+\frac{1}{2m^4}Q_1^4Q_2^6+Q_1^6-3Q_1^4Q_2^2-Q_1^2Q_2^4+Q_2^6\right]\left(1-\frac{R_1^m}{Q_1^2}\right) \\
& -\left(Q_1^2-Q_2^2\right)^2R^0\left(1-\frac{R_1^m}{Q_1^2}\right)+\frac{1}{m^2}Q_2^2\left(Q_2^4-4m^4\right)R_1^m \\
& -\frac{1}{2m^4}Q_1^4\left(Q_2^2-2m^2\right)^2R_2^m+\frac{1}{2m^4}\left(Q_2^2-2m^2\right)\left(Q_1^2Q_2^2-2m^2Q_1^2-2m^2Q_2^2\right)R_1^mR_2^m\Bigg\}
\end{aligned}
\tag{2.35}
$$

$$
\begin{aligned}
w_{g_1}(M,Q_1,Q_2) = {} & \frac{\pi^2}{Q_2^2+M_\pi^2}\frac{1}{6m^2Q_1Q_2}\Bigg\{-4\left(2m^2-Q_2^2\right)\left(Q_1^2-Q_2^2\right)^2 \\
& \times\ln\left[1+\frac{\left(Q_1^2+Q_2^2-R^0\right)\left(Q_1^2-R_1^m\right)\left(Q_2^2-R_2^m\right)}{8m^2Q_1^2Q_2^2}\right] \\
& +4\left(2m^2-Q_2^2\right)\left[M^4+\left(Q_1^2-Q_2^2\right)^2+2M^2\left(Q_1^2+Q_2^2\right)\right] \\
& \times\ln\left[1+\frac{\left(M^2+Q_1^2+Q_2^2-R^M\right)\left(Q_1^2-R_1^m\right)\left(Q_2^2-R_2^m\right)}{8m^2Q_1^2Q_2^2}\right] \\
& -\left[M^6+3M^4Q_1^2+3M^2Q_1^4+3M^4Q_2^2+2M^2Q_1^2Q_2^2+3M^2Q_2^4-\frac{M^2}{m^2}Q_1^2Q_2^4\right]\left(1-\frac{R_1^m}{Q_1^2}\right) \\
& -\left(Q_1^2-Q_2^2\right)^2R^0\left(1-\frac{R_1^m}{Q_1^2}\right)-\frac{M^2}{m^2}Q_1^2\left(Q_2^2-2m^2\right)R_2^m\left(1-\frac{R_1^m}{Q_1^2}\right) \\
& +[M^4+2M^2Q_1^2+2M^2Q_2^2+Q_1^4+Q_2^4-2Q_1^2Q_2^2]R^M\left(1-\frac{R_1^m}{Q_1^2}\right)\Bigg\}
\end{aligned}
\tag{2.36}
$$

$$
\begin{aligned}
w_{g_2}(M,Q_1,Q_2) = \frac{\pi^2}{6m^2M^2Q_1Q_2}\Bigg\{ & 4\left[m^2\left(Q_2^2-Q_1^2\right)+2Q_1^2Q_2^2\right]\left(Q_1^2-Q_2^2\right) \\
& \times \ln\left[1+\frac{\left(Q_1^2+Q_2^2-R^0\right)\left(Q_1^2-R_1^m\right)\left(Q_2^2-R_2^m\right)}{8m^2Q_1^2Q_2^2}\right] \\
& + 4\Big[M^4m^2+\left(Q_1^2-Q_2^2\right)\left[-2Q_1^2Q_2^2+m^2\left(Q_1^2-Q_2^2\right)\right]+2M^2\left[Q_1^2Q_2^2+m^2\left(Q_1^2+Q_2^2\right)\right]\Big] \\
& \times \ln\left[1+\frac{\left(M^2+Q_1^2+Q_2^2-R^M\right)\left(Q_1^2-R_1^m\right)\left(Q_2^2-R_2^m\right)}{8m^2Q_1^2Q_2^2}\right] \\
& + M^4Q_1^2+2M^2Q_1^4+M^4Q_2^2-M^2Q_1^2Q_2^2+2M^2Q_2^4+Q_1^2\left(Q_1^2+Q_2^2\right)R^0\left(1-\frac{R_1^m}{Q_1^2}\right) \\
& + Q_2^2\left(Q_2^2-3Q_1^2\right)R^0\left(1-\frac{R_2^m}{Q_2^2}\right)-Q_1^2\left(M^2+Q_1^2+Q_2^2\right)R^M\left(1-\frac{R_1^m}{Q_1^2}\right) \\
& - M^2\left(M^2+2Q_1^2+Q_2^2\right)R_1^m-Q_2^2\left(M^2-3Q_1^2+Q_2^2\right)R^M\left(1-\frac{R_2^m}{Q_2^2}\right) \\
& - M^2\left(M^2-3Q_1^2+2Q_2^2\right)R_2^m-M^2R_1^mR_2^m\Bigg\}
\end{aligned}
\tag{2.37}
$$

where $m = m_\mu = 105.66\ MeV$ is the mass of the muon and

$$R^M = \sqrt{\left(M^2+Q_1^2+Q_2^2\right)^2-4Q_1^2Q_2^2} \tag{2.38}$$

$$R^0 \equiv R^{M=0} = \sqrt{\left(Q_1^2+Q_2^2\right)^2-4Q_1^2Q_2^2} \tag{2.39}$$

$$R_i^m = \sqrt{Q_i^4+4m^2Q_i^2}, \quad i=1,2 \tag{2.40}$$

Although the analytical expressions for the weight functions look quite complicated and involve terms with different signs and of different sizes, the sum of all terms leads to rather smooth functions of the two variables Q_1 and Q_2. We will see the corresponding plots when we present the results in Chap. 3. Notice that we have reduced a eight-dimensional integral (2.18) to a two-dimensional integral over the moduli of the Euclidean loop momenta (2.28).

2.3 Other contributions

As mentioned in Sect. 2.1.1, the HLbL scattering can be split into a set of different contributions: the pion-exchange contribution (dominant), exchanges of axial-vector mesons, exchanges of scalar mesons, exchanges of tensor mesons, the charged pion and kaon loops, and the quark-loop. Each one of them, requires a thorough discussion.

In our thesis we have focused on the pion-exchange contribution in the pion-pole approach. Thanks to Knecht and Nyffeler [43] we were able to reduce the eight dimensional two-loop integral into a two-dimensional integral, which can be computed numerically without real problems. Nevertheless, this is not the case for the

other contributions, not even for the pion-exchange contribution without pion-pole approximation. In general, for the pion-exchange contribution one ends up with a three-dimensional integral with different weight functions and products of two form factors with off-shell pions. Such form factors require descriptions different from those discussed here.

For the exchanges of axial-vector, scalar and tensor mesons we can also obtain a three-dimensional integral, but we have to replace the pseudoscalar mesons and the form factors by the corresponding expressions. Furthermore, the weight functions must be deduced again. For more information, see [40].

The simplest model to compute the charged pion or kaon loop is scalar QED (sQED) exhibiting 6 box diagrams, 12 triangle diagrams and 3 bulb diagrams (see Fig. 2.6). Considering the mixing between $\gamma^* - \rho^0$, the sQED contribution gets modified to

$$\Pi^{\mu\nu\lambda\sigma}_{\text{sQED+VMD}} = F_\pi^V\left(q_1^2\right) F_\pi^V\left(q_2^2\right) F_\pi^V\left(q_3^2\right) F_\pi^V\left(q_4^2\right) \Pi^{\mu\nu\lambda\sigma}_{\text{sQED}} \tag{2.41}$$

where $F_\pi^V\left(q^2\right)$ is the pion form factor. More recently, it has been argued that the effect of pion polarizability has been missing in earlier calculations and that the effects could be sizeable. For more information, we encourage reading [25, 33, 1].

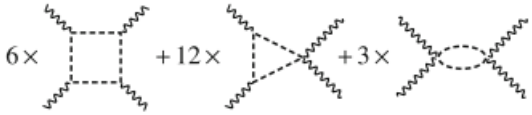

FIGURE 2.6: Contributions to $ie^4\Pi^{\mu\nu\lambda\sigma}_{\text{sQED}}$. Adapted from [40].

As mentioned in Sect. 2.1.1, the quark loops including hard gluonic corrections dominate at short distances (S.D.). Therefore, we expect a contribution evaluated from the perturbative QCD (pQCD) expansion. This hard region is separated from the soft region by a cut-off in the GeV range. This generally results in a substantial cut-off dependence of the results. However, whether a quark-loop contribution has to be taken into account or not depends on the framework in which one is evaluating the HLbL contribution. Particularly, in the large-N_c approach, a separate quark loop is absent unless one applies a cut-off to separate both regions, which however is not in the spirit of such approach [40].

For more information about two photon physics concerning the two photon production to mesons as well as the two photon coupling to mesons, see [58]. There you can find the formalism and the available data for the $\gamma^*\gamma^* \to$ meson transition form factors, and successively discuss the C-even pseudo-scalar ($J^{PC} = 0^{-+}$), scalar ($J^{PC} = 0^{++}$), axial-vector ($J^{PC} = 1^{++}$), and tensor ($J^{PC} = 2^{++}$) mesons.

2.4 Dual-Large N_c QCD model

In its original formulation, Vector Meson Dominance (VMD) is an effective tree-level model based on the $\gamma - \rho^0$ mixing. If used to compute electromagnetic form factors, it can very roughly account for the pion form factor data in the space-like region, and with some modifications (unitarization), also in the time-like region around the rho-meson peak. However, for non-zero spin hadrons such as nucleons and $\Delta(1236)$, VMD is in serious disagreement with the observed q^2 fall-off of these form factors. It has been generally believed that the reason for this discrepancy is that the radial

excitations of the ρ-meson are not taken into account in naive VMD. In fact, an infinite sum of monopole terms with suitable coefficients can lead to a form factor with an asymptotic behavior different from a monopole. An attempt to remedy this situation was made long ago by incorporating radial excitations of the rho-meson into VMD, the so-called Extended VMD (EVMD) [30]. At that time, though, there was no known renormalizable QFT to support this approach. Today, we know that in the limit of an infinite number of colors $N_c \to \infty$, QCD is solvable and leads to an hadronic spectrum consisting of an infinite number of zero-width states [4]. However, the masses and couplings of these states remain unspecified, so that models are needed to fix these parameters. An attractive and highly economical candidate is the Dual-Large N_c QCD model (Dual-QCD_∞), inspired in the Dual Resonance Model for scattering amplitudes of Veneziano [72], the precursor of string theory. It is important to stress that Dual-QCD_∞ is not intended to be an expansion in powers of $1/N_c$. In fact, N_c is taken to be infinite from the start, as this is the limit in which QCD is solvable and leads to the hadronic spectrum mentioned above [24].

2.4.1 EVMD $\pi^0\gamma\gamma$ transition form factor

We extend the vector meson dominance (VMD) $\pi^0\gamma\gamma$ transition form factor by summing up the infinite number of zero-width resonances that appear in the large-N_c limit. In order to do so, the masses and couplings of the zero-width states are fixed so that the form factor becomes an Euler Beta function of the Veneziano type, involving one single free parameter which controls their asymptotic power behaviour. The choice here is the factorizable dual model for three-point functions in the zero-width approximation, whose expression for a general off-shell vertex is [21]

$$F\left(p_1^2, p_2^2, p_3^2\right) = g \prod_{i=1}^{3} \Gamma\left(\beta_i - s_i\right) \frac{\Gamma\left(-\alpha'\left(p_i^2 - M_i^2\right)\right)}{\Gamma\left(\beta_i - s_i - \alpha'\left(p_i^2 - M_i^2\right)\right)} \tag{2.42}$$

where the constant g is fixed by the value of the residue at the fully on-mass-shell point, $\alpha' = 1/2M_\rho^2$ is the Regge slope, s_i is the spin of the ith particle with

$$\alpha\left(p_i^2\right) = s_i + \alpha'\left(p_i^2 - M_i^2\right) \tag{2.43}$$

being the Regge trajectory, and β_i is a free parameter governing the asymptotic behaviour of the form factor in the space-like region.

The EVMD form factor is obtained comparing equation (2.42) to the VMD form factor (2.23). The pion has spin $s_1 = 0$ and is on-shell $p_1^2 = M_\pi^2$, so the first term in the product of (2.42) vanishes. Then, taking into account that the photons have spin $s_2, s_3 = 1$ and are off-shell, and fixing the constant g, we deduce that the EVMD form factor is obtained by the following modification of the VMD propagator,

$$\frac{1}{M_V^2 - q^2} \to \alpha'\Gamma(\beta - 1)\frac{\Gamma\left(-\alpha'\left(q^2 - M_V^2\right)\right)}{\Gamma\left(\beta - 1 - \alpha'\left(q^2 - M_V^2\right)\right)} \tag{2.44}$$

such that

$$\begin{aligned}\mathcal{F}_{\pi^0\gamma^*\gamma^*}^{EVMD}\left(q_1^2, q_2^2\right) = -\frac{N_C}{12\pi^2 F_\pi} &\frac{M_V^2\alpha'\Gamma(\beta-1)\Gamma\left(-\alpha'\left(q_1^2 - M_V^2\right)\right)}{\Gamma\left(\beta - 1 - \alpha'\left(q_1^2 - M_V^2\right)\right)} \\ &\times \frac{M_V^2\alpha'\Gamma(\beta-1)\Gamma\left(-\alpha'\left(q_2^2 - M_V^2\right)\right)}{\Gamma\left(\beta - 1 - \alpha'\left(q_2^2 - M_V^2\right)\right)}\end{aligned} \tag{2.45}$$

The form factor exhibits asymptotic power behaviour in the space-like region, i.e. [24]

$$\lim_{s\to-\infty} F(s) = \left(-\alpha' s\right)^{(1-\beta)} \tag{2.46}$$

from which one identifies the free parameter β as controlling this asymptotic behaviour. In fact, the parameter β in the ρ-meson propagator is the same as that determined from the pion-form-factor F_π data [20], i.e. $\beta_\rho = \beta_\pi = 2.33$. It should be noticed that the value $\beta = 2$ reduces the form factor to single rho-meson dominance (naive Vector Meson Dominance).

The predictions of radiative meson decay widths using the EVMD form factor are in reasonable agreement with the data and represent a considerable improvement over VMD results (see Fig. 2.7). Except possibly for $K^{*-} \to K^-\gamma$, the overall quality of the predictions is fairly good. It seems that the radial excitations of the ground-state vector meson give rise to sizeable corrections to naive VMD predictions. This provides additional evidence in support of the Dual-QCD_∞ model.

Decay	VMD	EVMD (a)	EVMD (b)	Experiment
$\pi^0 \to \gamma\gamma$ (eV)	16	8.3	7.3	8.0 ± 0.6
$\rho \to \pi\gamma$	129	92	87	68 ± 8
$\omega \to \pi\gamma$	1448	1025	966	861 ± 56
$\phi \to \pi\gamma$	6	5	4	6 ± 2
$\eta \to \gamma\gamma$	0.781	0.388	0.345	0.324 ± 0.047
$x \to \gamma\gamma$	13	6	5	5 ± 2
$\rho \to \eta\gamma$	91	63.5	60	55 ± 14
$\omega \to \eta\gamma$	12	8	8	3 ± 2.5
$X \to \rho\gamma$	194	137	129	84 ± 30
$X \to \omega\gamma$	18	12	12	8 ± 3
$\phi \to \eta\gamma$	290	57	55	63 ± 9
$K^{*0} \to K^0\gamma$	368	72	69	78 ± 36
$K^{*-} \to K^-\gamma$	90	18	17	62 ± 14
χ^2	1206	40	31	

FIGURE 2.7: Radiative meson decay widths in keV predicted by VMD and EVMD. Column (a) results from using factorization ($\beta_\rho = 2.33$) plus the assumption $\beta_\rho = \beta_w = \beta_\phi$. Column (b) is the result of a χ^2 fit to the data regarding these parameters as free, yielding $\beta_\rho = 2.4$, $\beta_w = 2.4$, and $\beta_\phi = 2.36$. Experimental data is taken from [5]. Adapted from [21].

In order to compute the pion-pole contribution to a_μ with the EVMD $\pi^0\gamma\gamma$ transition form factor, we use equation (2.28) assuming the VMD model, but replacing $\mathcal{F}^{VMD}_{\pi^0\gamma^*\gamma^*}\left(q_1^2, q_2^2\right)$ by $\mathcal{F}^{EVMD}_{\pi^0\gamma^*\gamma^*}\left(q_1^2, q_2^2\right)$ and the propagator of the $g_{M_V}(q^2)$ function that comes from the general representation of the form factors (2.25). $f(q^2) \equiv 0$ for the VMD case (see Fig. 2.5).

2.4.2 ELMD $\pi^0\gamma\gamma$ transition form factor

We proceed as we did for the EVMD case (see Sect. 2.4.1). The ELMD form factor is obtained by the same modification of the propagator (see equation (2.44)), such that

$$\begin{aligned}\mathcal{F}^{ELMD}_{\pi^0\gamma^*\gamma^*}\left(q_1^2,q_2^2\right) = \frac{F_\pi}{3}\left(q_1^2+q_2^2-\frac{N_C}{4\pi^2}\frac{M_V^4}{F_\pi^2}\right)\frac{\alpha'\Gamma(\beta-1)\Gamma\left(-\alpha'\left(q_1^2-M_V^2\right)\right)}{\Gamma\left(\beta-1-\alpha'\left(q_1^2-M_V^2\right)\right)} \\ \times\frac{\alpha'\Gamma(\beta-1)\Gamma\left(-\alpha'\left(q_2^2-M_V^2\right)\right)}{\Gamma\left(\beta-1-\alpha'\left(q_2^2-M_V^2\right)\right)}\end{aligned} \tag{2.47}$$

In order to compute the pion-pole contribution to a_μ with the ELMD $\pi^0\gamma\gamma$ transition form factor, we use equation (2.28) assuming the LMD model, but replacing $\mathcal{F}^{LMD}_{\pi^0\gamma^*\gamma^*}\left(q_1^2,q_2^2\right)$ by $\mathcal{F}^{ELMD}_{\pi^0\gamma^*\gamma^*}\left(q_1^2,q_2^2\right)$ and the propagator of the $f(q^2)$ and $g_{M_V}(q^2)$ functions that come from the general representation of the form factors (2.25) (see Fig. 2.5).

2.4.3 EVMD $\eta\gamma\gamma$ and $\eta'\gamma\gamma$ transition form factors

So far we have not considered any model for the form factors of the light pseudoscalars η and η'. In such cases, it is not so straightforward to deduce $\mathcal{F}_{PS\gamma^*\gamma^*}\left(q_1^2,q_2^2\right)$, $PS=\eta,\eta'$. For the η, the effect of non-zero quark masses has definitely to be taken into account. Furthermore, the η' has a large admixture from the singlet state, and the gluonic contribution to the axial anomaly will play an important role. Here, we resort to a simplified approach and take a simple VMD form factor [56]

$$\mathcal{F}^{\text{VMD}}_{\text{PS}^*\gamma^*\gamma^*}\left(q_3^2,q_1^2,q_2^2\right) = -\frac{N_C}{12\pi^2 F_{\text{PS}}}\frac{M_V^2}{\left(q_1^2-M_V^2\right)}\frac{M_V^2}{\left(q_2^2-M_V^2\right)}, \quad \text{PS}=\eta,\eta' \tag{2.48}$$

normalized to the experimental decay width $\Gamma(\text{PS}\to\gamma\gamma)$. We can fix the normalization by adjusting the (effective) pseudoscalar decay constant F_{PS}: Using the latest values $\Gamma(\eta\to\gamma\gamma)=(0.516\pm0.026)\ keV$ and $\Gamma(\eta'\to\gamma\gamma)=(4.36\pm0.15)\ keV$ from [70], one obtains $F_{\eta,eff}=93.0\ MeV$ with $M_\eta=547.862\ MeV$ and $F_{\eta',eff}=74.0\ MeV$ with $M'_\eta=957.66\ MeV$.

The form factor described in equation (2.48) is off-shell. However, we are interested in the form factor with the pseudoscalar on-shell. The CLEO Collaboration [31] has made a fit of the on-shell form factors $\mathcal{F}_{PS\gamma^*\gamma^*}\left(q_1^2,q_2^2\right)$, $PS=\eta,\eta'$ using a VMD Ansatz with an adjustable parameter Λ_{PS} in place of the vector-meson mass M_V,

$$\mathcal{F}^{\text{VMD}}_{\text{PS}\gamma^*\gamma^*}\left(q_1^2,q_2^2\right) = -\left|\frac{1}{(4\pi\alpha)^2}\frac{64\pi\Gamma(\mathcal{PS}\to\gamma\gamma)}{M_{PS}^3}\right|^{1/2}\frac{\Lambda_{PS}^2}{\left(q_1^2-\Lambda_{PS}^2\right)}\frac{\Lambda_{PS}^2}{\left(q_2^2-\Lambda_{PS}^2\right)} \tag{2.49}$$

where $\Lambda_\eta=(774\pm29)\ MeV$ and $\Lambda_{\eta'}=(859\pm28)\ MeV$ [31].

In order to extend the VMD $\eta\gamma\gamma$ and $\eta'\gamma\gamma$ transition form factors, we proceed as we did for the EVMD $\pi^0\gamma\gamma$ case (see Sect. 2.4.1), i.e. it is obtained by the same modification of the propagator (see equation (2.44)), such that

$$\begin{aligned}\mathcal{F}^{\text{EVMD}}_{\text{PS}\gamma^*\gamma^*}\left(q_1^2,q_2^2\right) = -\left|\frac{1}{(4\pi\alpha)^2}\frac{64\pi\Gamma(\mathcal{PS}\to\gamma\gamma)}{M_{PS}^3}\right|^{1/2}\frac{\Lambda_{\text{PS}}^2\alpha'\Gamma(\beta-1)\Gamma\left(-\alpha'\left(q_1^2-\Lambda_{\text{PS}}^2\right)\right)}{\Gamma\left(\beta-1-\alpha'\left(q_1^2-\Lambda_{\text{PS}}^2\right)\right)} \\ \times\frac{\Lambda_{\text{PS}}^2\alpha'\Gamma(\beta-1)\Gamma\left(-\alpha'\left(q_2^2-\Lambda_{\text{PS}}^2\right)\right)}{\Gamma\left(\beta-1-\alpha'\left(q_2^2-\Lambda_{\text{PS}}^2\right)\right)}, \quad \text{PS}=\eta,\eta'\end{aligned} \tag{2.50}$$

The computation of the η-pole and η'-pole contributions to a_μ with the EVMD $\eta\gamma\gamma$ and $\eta'\gamma\gamma$ transition form factors is performed using equation (2.28) assuming the VMD model, but replacing $\mathcal{F}^{VMD}_{\pi^0\gamma^*\gamma^*}\left(q_1^2, q_2^2\right)$ by $\mathcal{F}^{EVMD}_{\eta\gamma^*\gamma^*}\left(q_1^2, q_2^2\right)$, $\mathcal{F}^{EVMD}_{\eta'\gamma^*\gamma^*}\left(q_1^2, q_2^2\right)$ and the propagator of the $g_{M_V}(q^2)$ function that comes from the general representation of the form factors (2.25) (see Fig. 2.5). Notice, we no longer have the same $g_{M_V}(q^2)$ as in the VMD pion case, instead

$$g_{M_V}(q^2) = -\left|\frac{1}{(4\pi\alpha)^2}\frac{64\pi\Gamma(\mathcal{PS}\to\gamma\gamma)}{M_{PS}^3}\right|^{1/2}\frac{3}{F_\pi}\frac{\Lambda_{\rm PS}^4}{q^2-\Lambda_{\rm PS}^2}. \tag{2.51}$$

We also need to replace all the M_π by M_η, M'_η.

2.4.4 EVMD electromagnetic form factor of the pion

As mentioned in Sect. 2.3, the pion form factor appears in the discussion of the charged pion loop, which is not considered in this thesis. Nevertheless, we want to represent such form factor using the Dual-QCD_∞ model.

With the standard definition of the pion form factor [22]

$$\left\langle \pi\left(p_2\right)\left|J_\mu^{EM}\right|\pi\left(p_1\right)\right\rangle = \left(p_1+p_2\right)_\mu F_\pi(s) \tag{2.52}$$

where $s \equiv q^2 = \left(p_2-p_1\right)^2$ is the momentum transfer squared, one expects that in the limit $N_c \to \infty$, the form factor presents the generic form [23]

$$F(s) = \sum_{n=0}^{\infty}\frac{C_n}{\left(M_n^2-s\right)} \tag{2.53}$$

where the masses M_n and the couplings C_n remain unspecified. The purpose of our model is to use a specific choice of masses and couplings in order to obtain an Euler's Beta function type form factor. The coefficients C_n are chosen as

$$C_n = \frac{\Gamma(\beta-1/2)}{\alpha'\sqrt{\pi}}\frac{(-1)^n}{\Gamma(n+1)}\frac{1}{\Gamma(\beta-1-n)} \tag{2.54}$$

where β is the free parameter governing the asymptotic behaviour of the form factor in the space-like region ($s<0$), and $\alpha' = 1/2M_\rho^2$ is the universal string tension entering the rho-meson Regge trajectory

$$\alpha_\rho(s) = 1+\alpha'\left(s-M_\rho^2\right). \tag{2.55}$$

The parameter β can be fitted from data using equation (2.46). Alternatively, β can be determined from the measured mean squared radius of the pion [24]. On the other hand, the mass spectrum is chosen as

$$M_n^2 = M_\rho^2(1+2n) \tag{2.56}$$

This simple formula correctly predicts the first few radial excitations. Other, e.g. non-linear mass formulas could be used, but this hardly changes the results in the space-like region, and only affects the time-like region behaviour for very large q^2.

The electromagnetic form factor of the pion obtained considering this particular realization of QCD in the large N_c limit becomes an Euler Beta-function,

$$\begin{aligned} F(s) &= \frac{\Gamma(\beta - 1/2)}{\sqrt{\pi}} \sum_{n=0}^{\infty} \frac{(-1)^n}{\Gamma(n+1)} \frac{1}{\Gamma(\beta - 1 - n)} \frac{1}{[n + 1 - \alpha_\rho(s)]} \\ &= \frac{1}{\sqrt{\pi}} \frac{\Gamma(\beta - 1/2)}{\Gamma(\beta - 1)} B\left(\beta - 1, 1/2 - \alpha' s\right) \end{aligned} \tag{2.57}$$

where $B(x, y) = \Gamma(x)\Gamma(y)/\Gamma(x + y)$ is the Euler Beta function. Once again, for $\beta = 2$ one recovers the VMD result. The form factor (2.57) is shown in Fig. 2.8, together with the available experimental data in the space-like region and the VMD prediction. The EVMD form factor agrees with space-like data much better than single rho-meson dominance.

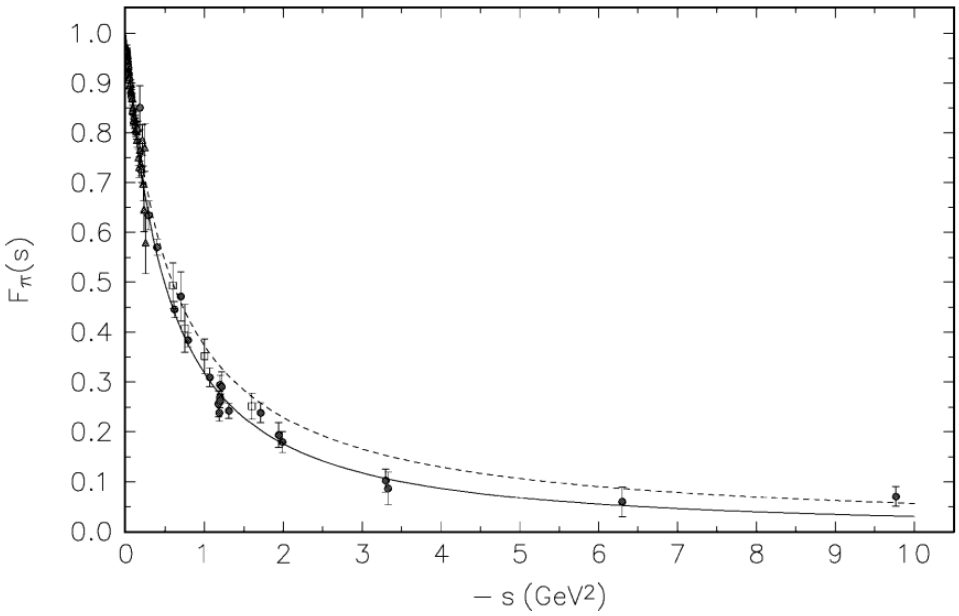

FIGURE 2.8: EVMD electromagnetic form factor (2.57) in the space like region for the least-squared fitted parameter $\beta = 2.33$ (solid curve), together with the naive VMD ($\beta = 2$) (dash curve), and the experimental data. Adapted from [22].

Chapter 3

Results

This chapter presents the results of the thesis and discuss its behaviour. We follow the methodology introduced in Chap. 2. As mentioned in Sect. 2.2, the pseudoscalar-pole contribution to a_μ is computed from equation 2.28, which consists of a two-dimensional integral over the moduli of the Euclidean loop momenta that can be computed numerically [1] without real problems. Such expression is described in terms of the form factors and several weight functions. As a consequence, the result rely on the pseudoscalar considered and the hadronic model used to represent the form factor.

We split the results as: π^0-pole contribution, η-pole contribution and η'-pole contribution. For each one, we show the corresponding weight functions (2.35), (2.36) and (2.37), since w depends on the mass of the pseudoscalar. We also show the form factors used, deduced from the Dual-Large N_c QCD model (see Sect. 2.4). The results of the contributions are shown as a function of a cut-off Λ in the loop momenta in order to distinguish the most contributing regions. Only when the cut-off exceeds about 2 GeV, the result a_μ is well approximated. These three mentioned contributions, correspond to the lowest-mass part of $\Pi_{\mu\nu\lambda\rho}$ that is leading in the large-N_c limit, which might provide an explanation as to why it happens to constitute the dominant fraction of the light-by-light scattering correction to a_μ. The sum of the three light pseudoscalar poles gives the pseudoscalar-pole contribution. We compare our findings with those of other references.

3.1 π^0-pole contribution

We compute the π^0-pole contribution with the EVMD (2.45) and the ELMD (2.47) form factors. The EVMD model involves the w_{g_1} and w_{g_2} weight functions, while the ELMD model also requires w_{f_1}. We have used the following input values: The mass of the muon $m = m_\mu = 105.66\ MeV$, the mass of the pion $M_\pi = 134.98\ MeV$, the fine-structure constant $\alpha = 1/137.03599976$, the pion decay constant $F_\pi = 92.4\ MeV$, the rho vector meson $M_V = M_\rho = 769\ MeV$, the number of colours in QCD $N_c = 3$, the Regge slope $\alpha' = 1/2M_V^2$ and the free parameter $\beta_\rho = 2.33$ [70].

The weight functions are shown in Fig. 3.1. As observed, although the analytical expressions for the weight functions look quite complicated and involve terms with different signs and of different sizes, the sum of all terms leads to rather smooth functions of the two variables Q_1 and Q_2. The functions w_{f_1} and w_{g_1} are positive definite and peaked in the region $Q_1 \approx Q_2 \approx 0.5\ GeV$. Note, however, the tail in w_{f_1} in the Q_1 direction for $Q_2 \approx 0.2\ GeV$. The functions $w_{g_2}(Q_1, Q_2, M_\pi)$ and $w_{g_2}(Q_1, Q_2, M_\rho)$ take both signs, which will lead to a strong cancellation in the corresponding integrals, provided they are multiplied by a positive function composed

[1] All numerical evaluations and plots are performed using Python.

of the form factors. Nevertheless, their magnitudes remain small as compared to $w_{f_1}(Q_1, Q_2, M_\pi)$ and $w_{g_1}(Q_1, Q_2, M_\rho, M_\pi)$.

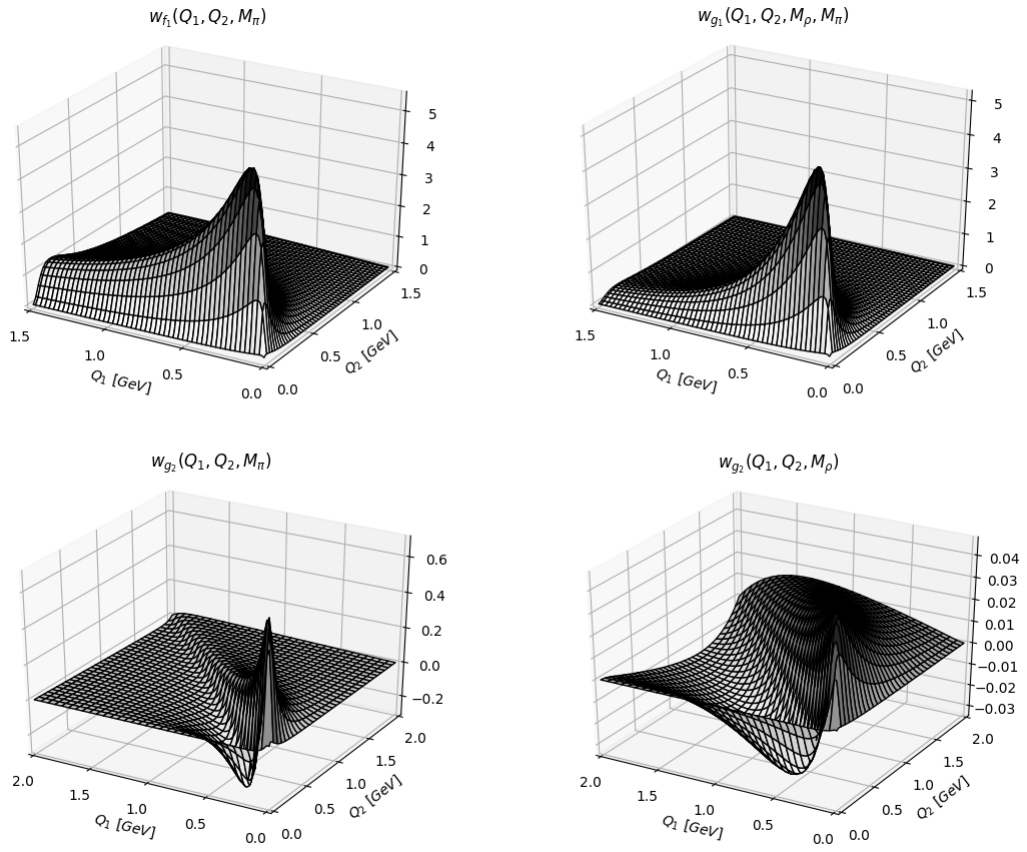

FIGURE 3.1: Weight functions of equations (2.35)-(2.37) for the π^0-pole contribution. Notice the difference in scales and ranges of Q_i.

As can be seen from the plots, and checked analytically, the weight functions vanish for small momenta. Therefore, the integrals are infrared finite. For large momenta, the weight functions have the following behaviour:

$$\lim_{Q_1\to\infty} w_{f_1}(Q_1, Q_2, M_\pi) = \pi^2 \frac{\left[Q_2^5 - Q_2\left(Q_2^2 - 2m^2\right) R_2^m\right]}{m^2\left(Q_2^2 + M_\pi^2\right) Q_1} + \mathcal{O}\left(\frac{1}{Q_1^3}\right), \quad Q_2 \text{ fixed} \tag{3.1}$$

$$\lim_{Q_2\to\infty} w_{f_1}(Q_1, Q_2) = \pi^2 \frac{\left[2Q_1^3\left(Q_1^2 - 12m^2\right) - 2Q_1\left(Q_1^2 - 14m^2\right) R_1^m\right]}{9m^2 Q_2^3} + \mathcal{O}\left(\frac{1}{Q_2^5}\right), \quad Q_1 \text{ fixed} \tag{3.2}$$

$$\lim_{Q\to\infty} w_{f_1}(Q, Q) = \pi^2 \frac{13m^2}{3Q^2} + \mathcal{O}\left(\frac{1}{Q^4}\right) \tag{3.3}$$

$$\lim_{Q_1\to\infty} w_{g_1}\left(Q_1,Q_2,M,M_\pi\right) = \pi^2\frac{M^2\left[Q_2^5 - Q_2\left(Q_2^2-2m^2\right)R_2^m\right]}{m^2\left(Q_2^2+M_\pi^2\right)Q_1^3} + \mathcal{O}\left(\frac{1}{Q_1^5}\right), \quad Q_2 \text{ fixed} \tag{3.4}$$

$$\lim_{Q_2\to\infty} w_{g_1}\left(Q_1,Q_2,M\right) = \pi^2\frac{M^2\left[-18m^2Q_1^3 + 5Q_1^5 + Q_1\left(28m^2-5Q_1^2\right)R_1^m\right]}{9m^2Q_2^5} + \mathcal{O}\left(\frac{1}{Q_2^7}\right), \quad Q_1 \text{ fixed} \tag{3.5}$$

$$\lim_{Q\to\infty} w_{g_1}(Q,Q,M) = \pi^2\frac{22M^2m^2}{3Q^4} + \mathcal{O}\left(\frac{1}{Q^5}\right) \tag{3.6}$$

$$\lim_{Q_1\to\infty} w_{g_2}\left(Q_1,Q_2,M\right) = \pi^2\frac{\left[-Q_2^3\left(Q_2^2+m^2\right) + Q_2\left(Q_2^2-m^2\right)R_2^m\right]}{3m^2Q_1^3} + \mathcal{O}\left(\frac{1}{Q_1^5}\right), \quad Q_2 \text{ fixed} \tag{3.7}$$

$$\lim_{Q_2\to\infty} w_{g_2}\left(Q_1,Q_2,M\right) = \pi^2\frac{\left[-Q_1^3\left(Q_1^2+5m^2\right) + Q_1\left(Q_1^2+3m^2\right)R_1^m\right]}{3m^2Q_2^3} + O\left(\frac{1}{Q_2^5}\right), \quad Q_1 \text{ fixed} \tag{3.8}$$

$$\lim_{Q\to\infty} w_{g_2}(Q,Q) = \pi^2\frac{16m^4}{9Q^4} + \mathcal{O}\left(\frac{1}{Q^5}\right) \tag{3.9}$$

The EVMD and ELMD form factors are shown in Fig. 3.2 and 3.3. They are both compared with their non-extended form factors, VMD (2.23) and LMD (2.23) respectively. According to experiments [15], the form factor $\mathcal{F}_{\pi^0\gamma^*\gamma}(-Q^2,0)$ with one photon on-shell behaves as

$$\lim_{Q^2\to\infty} \mathcal{F}_{\pi^0\gamma^*\gamma}\left(m_\pi^2,-Q^2,0\right) \sim \frac{2F_\pi}{Q^2} \tag{3.10}$$

where $Q^2 = -q^2$. As observed in Fig. 3.2, the VMD form factor presents a damping too strong, since $\mathcal{F}^{VMD}_{\pi^0\gamma^*\gamma}\left(m_\pi^2,-Q^2,0\right) \sim 1/Q^4$. However, the EVMD form factor exhibits an even stronger damping. This effect might lead to an underestimating of the contribution to a_μ. As observed in Fig. 3.3, neither the LMD nor the ELMD presents the expected asymptotic behaviour. In this case, the effect might lead to an

overestimated contribution. It should be noticed that the value $\beta = 2$ reduces the EVMD and ELMD form factors to one vector resonance, VMD and LMD respectively.

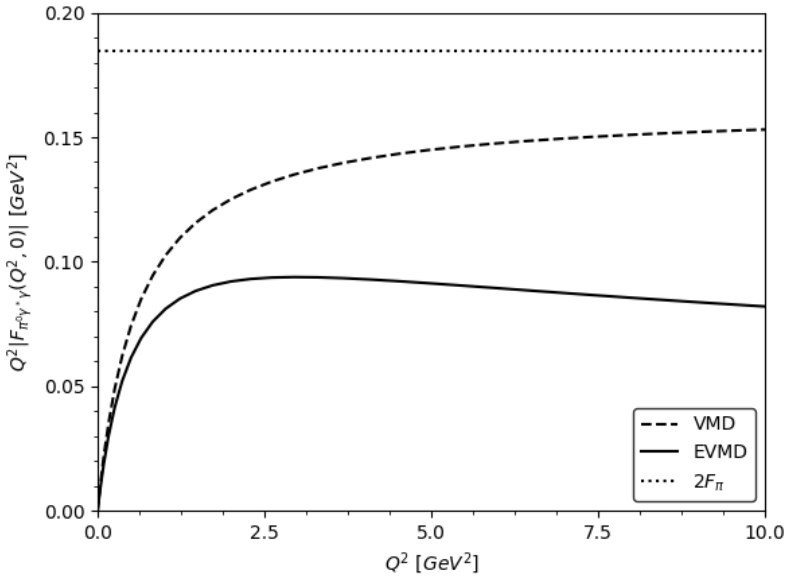

FIGURE 3.2: Comparison between the VMD (2.23) (dashed curve) and EVMD (2.45) (solid curve) form factors, together with the asymptotic expected behaviour (3.10) (dotted curve) for the π^0-pole contribution.

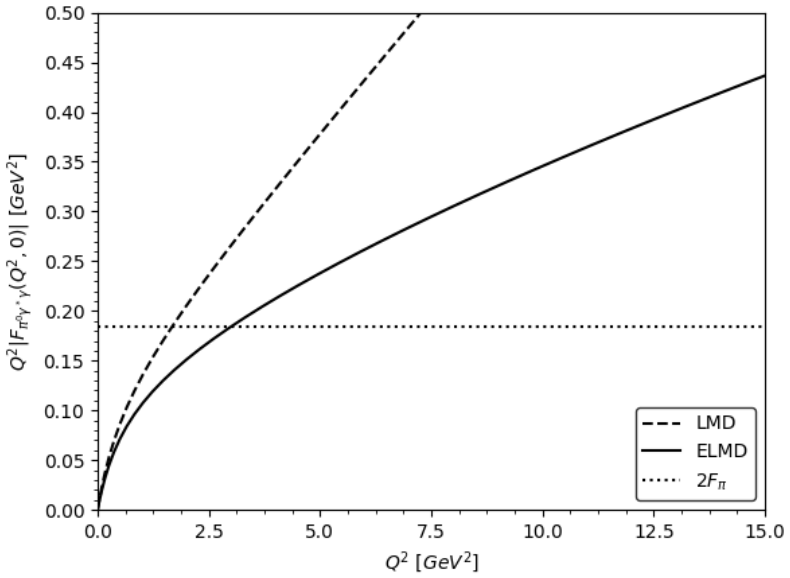

FIGURE 3.3: Comparison between the LMD (2.24) (dashed curve) and ELMD (2.47) (solid curve) form factors, together with the asymptotic expected behaviour (3.10) (dotted curve) for the π^0-pole contribution.

The results of the π^0-pole contribution (2.28) using the EVMD and ELMD form factors are shown in Tables 3.1 and 3.2 respectively. They are shown as a function of a cut-off Λ in the loop momenta in order to distinguish the most contributing regions. Only when the cut-off exceeds about 2 GeV, the result a_μ stabilizes. As expected from the plots of the weight functions (see Fig. 3.1), it is mainly the region $Q_i \leq 1\ GeV$ that contributes in the integrals.

Λ [GeV]	$a_\mu^{LbL;\pi^0(1)}$	$a_\mu^{LbL;\pi^0(2)}$	$a_\mu^{LbL;\pi^0} \times 10^{-10}$
0.5	0.0222	0.00096	2.907
0.7	0.0280	0.00101	3.638
1.0	0.0317	0.00103	4.106
2.0	0.0339	0.00104	4.369
4.0	0.0340	0.00104	4.390
6.0	0.0340	0.00104	4.391
10.0	0.0340	0.00104	4.392

TABLE 3.1: Results of the π^0-pole contribution (2.28) using the $\mathcal{F}^{EVMD}_{\pi^0\gamma^*\gamma^*}\left(q_1^2, q_2^2\right)$ form factor (2.45) as a function of a cut-off Λ in the loop momenta.

Λ [GeV]	$a_\mu^{LbL;\pi^0(1)}$	$a_\mu^{LbL;\pi^0(2)}$	$a_\mu^{LbL;\pi^0} \times 10^{-10}$
0.5	0.0240	0.00100	3.134
0.7	0.0314	0.00107	4.064
1.0	0.0370	0.00110	4.777
2.0	0.0418	0.00111	5.380
4.0	0.0429	0.00111	5.510
6.0	0.0430	0.00111	5.528
10.0	0.0431	0.00111	5.535

TABLE 3.2: Results of the π^0-pole contribution (2.28) using the $\mathcal{F}^{ELMD}_{\pi^0\gamma^*\gamma^*}\left(q_1^2, q_2^2\right)$ form factor (2.47) as a function of a cut-off Λ in the loop momenta.

Considering the saturated values from Tables 3.1 and 3.2, our estimations for the π^0-pole contribution are

$$a_{\mu\ EVMD}^{LbL;\pi^0} = (4.4 \pm 1.0) \times 10^{-10} \tag{3.11}$$

$$a_{\mu\ ELMD}^{LbL;\pi^0} = (5.5 \pm 1.0) \times 10^{-10}. \tag{3.12}$$

where the error includes the variation of the parameters and the intrinsic model dependence. The errors from the numerical integration are much smaller.

In comparison, we give the values obtained by Knecht and Nyffeler [43] using the VMD and LMD form factors,

$$a_{\mu\ VMD}^{LbL;\pi^0} = (5.6 \pm 1.0) \times 10^{-10} \tag{3.13}$$

$$a_{\mu\ LMD}^{LbL;\pi^0} = (7.3 \pm 1.0) \times 10^{-10}. \tag{3.14}$$

We also give its best result obtained using the LMD + V form factor [43],

$$a_{\mu\ LMD+V}^{LbL;\pi^0} = (5.8 \pm 1.0) \times 10^{-10}. \tag{3.15}$$

As observed, both of our results are underestimated with respect to the Knecht and Nyffeler fit. The reason arises from the form factor plots (see Fig. 3.2 and 3.3). In both cases, EVMD and ELMD, the form factor is smaller than the corresponding non-extended version. Consequently, the contribution to a_μ is smaller too.

3.2 η-pole contribution

We compute the η-pole contribution with the EVMD (2.50) form factor. We have used the following input values: The mass of the muon $m = m_\mu = 105.66\ MeV$, the mass of the eta meson $M_\eta = 547.862\ MeV$, the fine-structure constant $\alpha = 1/137.03599976$, the eta decay constant $F_\eta = 93\ MeV$, the adjustable parameter $\Lambda_\eta = 774\ MeV$ in place of the vector-meson mass M_V, the number of colours in QCD $N_c = 3$, the Regge slope $\alpha' = 1/2M_V^2$ and the free parameter $\beta_\rho = 2.33$ [70].

The weight functions are shown in Fig. 3.4. The EVMD model only involves w_{g_1} and w_{g_2}. Since we have changed the pseudoscalar and the vector-meson masses, they look a bit different with respect to the pion case. Notice the smaller scales of the weight functions, which lead to a smaller contribution to a_μ. Despite this, the shapes and behaviours are basically the same.

The EVMD form factor is shown in Fig. 3.5. It is compared with its non-extended form factor VMD (2.23) and the asymptotic expected behaviour (3.10). Again, we observe that the strong damping in the VMD form factor is boosted in the EVMD model.

The results of the η-pole contribution (2.28) using the EVMD form factor are shown in Table 3.3. Again, only when the cut-off exceeds about 2 GeV, the result a_μ stabilizes. Considering the saturated value from Table 3.3, our estimation for the η-pole contribution is

$$a_{\mu\ EVMD}^{LbL;\eta} = (1.1 \pm 0.1) \times 10^{-10} \tag{3.16}$$

where the error only reflects the corresponding variation in Λ_η. The errors from the numerical integration are much smaller. In comparison, we give the value obtained by Knecht and Nyffeler [43] using the VMD form factor,

$$a_{\mu\ VMD}^{LbL;\eta} = (1.3 \pm 0.1) \times 10^{-10} \tag{3.17}$$

Again, our result is underestimated with respect to the Knecht and Nyffeler fit. The reason arises from the form factor plot (see Fig. 3.5). The form factor is smaller than the corresponding non-extended version. However, we also have noticed that the eta decay constant used by Knecht and Nyffeler is less updated than ours.

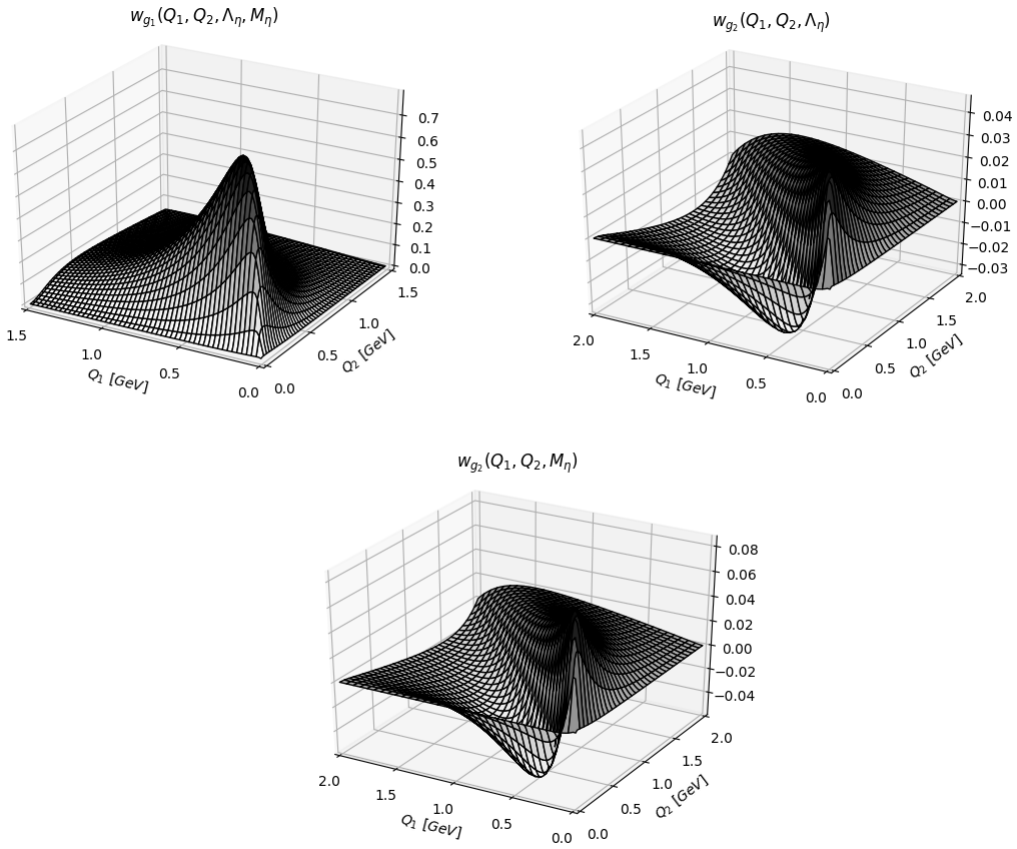

FIGURE 3.4: Weight functions of equations (2.36)-(2.37) for the η-pole contribution. Notice the difference in scales and ranges of Q_i.

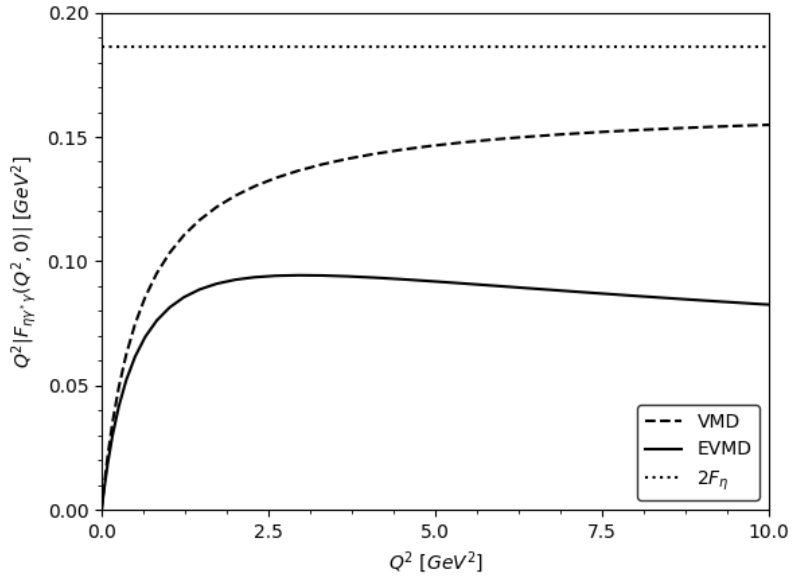

FIGURE 3.5: Comparison between the VMD (2.23) (dashed curve) and EVMD (2.50) (solid curve) form factors, together with the asymptotic expected behaviour (3.10) (dotted curve) for the η-pole contribution.

Λ [GeV]	$a_\mu^{LbL;\eta(1)}$	$a_\mu^{LbL;\eta(2)}$	$a_\mu^{LbL;\eta} \times 10^{-10}$
0.5	0.00427	0.000173	0.557
0.7	0.00623	0.000198	0.806
1.0	0.00772	0.000210	0.994
2.0	0.00865	0.000213	1.111
4.0	0.00873	0.000214	1.121
6.0	0.00874	0.000214	1.122
10.0	0.00874	0.000214	1.122

TABLE 3.3: Results of the η-pole contribution (2.28) using the $\mathcal{F}^{EVMD}_{\eta'\gamma^*\gamma^*}\left(q_1^2, q_2^2\right)$ form factor (2.50) as a function of a cut-off Λ in the loop momenta.

3.3 η'-pole contribution

We compute the η'-pole contribution with the EVMD (2.50) form factor. We have used the following input values: The mass of the muon $m = m_\mu = 105.66\ MeV$, the mass of the eta prime meson $M'_\eta = 958\ MeV$, the fine-structure constant $\alpha = 1/137.03599976$, the eta prime decay constant $F'_\eta = 74\ MeV$, the adjustable parameter $\Lambda'_\eta = 859\ MeV$ in place of the vector-meson mass M_V, the number of colours in QCD $N_c = 3$, the Regge slope $\alpha' = 1/2M_V^2$ and the free parameter $\beta_\rho = 2.33$ [70].

The weight functions are shown in Fig. 3.6 and the EVMD form factor is shown in Fig. 3.7. We observe that the VMD form factor limit $Q^2 \to \infty$ is above the asymptotic expected behaviour (3.10).

The results of the η'-pole contribution (2.28) using the EVMD form factor are shown in Table 3.4. Again, only when the cut-off exceeds about 2 GeV, the result a_μ stabilizes. Considering the saturated value from Table 3.4, our estimation for the η'-pole contribution is

$$a_{\mu\ EVMD}^{LbL;\eta'} = (0.7 \pm 0.1) \times 10^{-10} \tag{3.18}$$

where the error only reflects the corresponding variation in Λ'_η. The errors from the numerical integration are much smaller. In comparison, we give the value obtained by Knecht and Nyffeler [43] using the VMD form factor,

$$a_{\mu\ VMD}^{LbL;\eta'} = (1.2 \pm 0.1) \times 10^{-10} \tag{3.19}$$

This time, our result is more underestimated with respect to the Knecht and Nyffeler fit, than the η-pole case. The reason is that the difference between the EVMD and VMD form factors is larger than the η-pole case (see Fig. 3.7). However, we also have noticed that the eta decay constant used by Knecht and Nyffeler is less updated than ours.

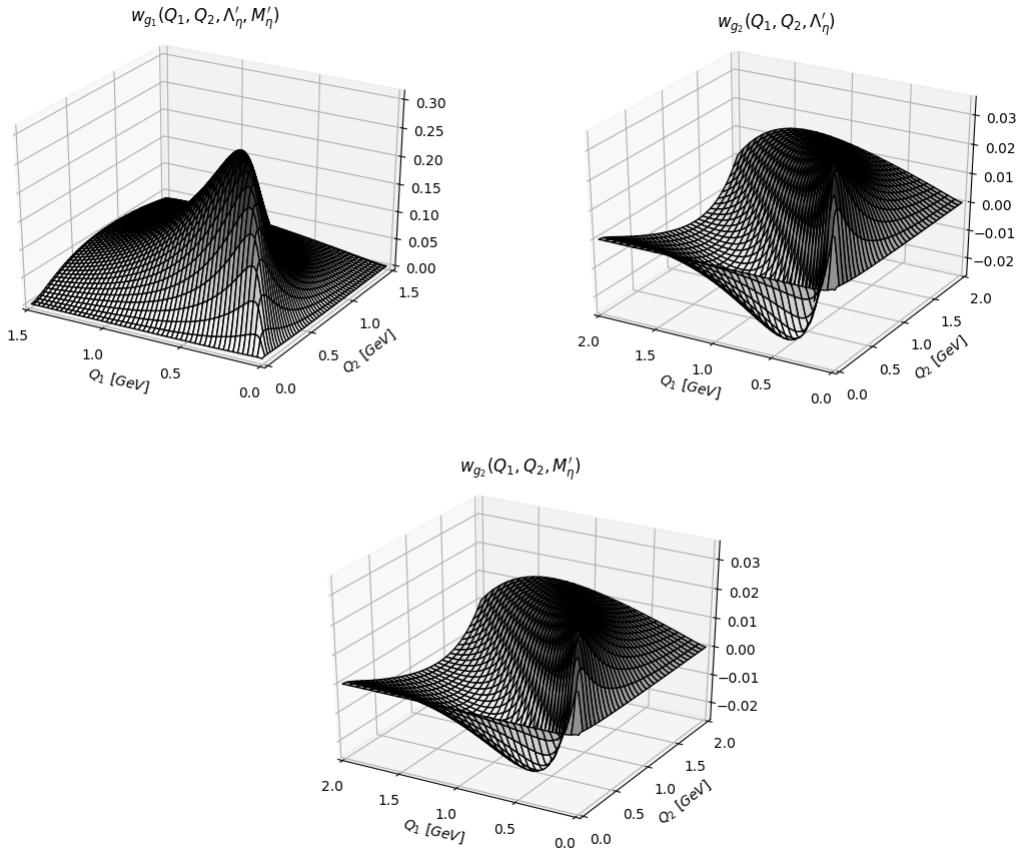

FIGURE 3.6: Weight functions of equations (2.36)-(2.37) for the η'-pole contribution. Notice the difference in scales and ranges of Q_i.

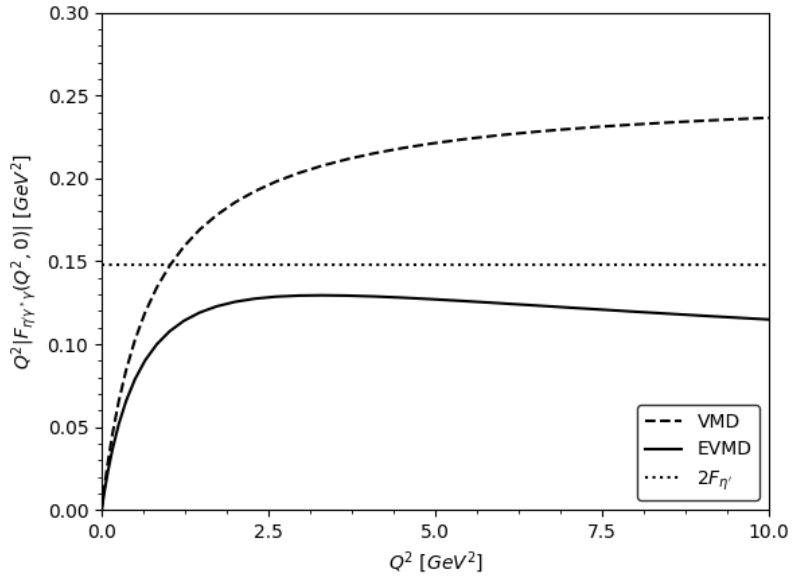

FIGURE 3.7: Comparison between the VMD (2.23) (dashed curve) and EVMD (2.50) (solid curve) form factors, together with the asymptotic expected behaviour (3.10) (dotted curve) for the η'-pole contribution.

Λ [GeV]	$a_\mu^{LbL;\eta'(1)}$	$a_\mu^{LbL;\eta'(2)}$	$a_\mu^{LbL;\eta'} \times 10^{-10}$
0.5	0.00201	0.000079	0.262
0.7	0.00322	0.000096	0.416
1.0	0.00434	0.000105	0.557
2.0	0.00520	0.000109	0.666
4.0	0.00529	0.000109	0.677
6.0	0.00529	0.000109	0.677
10.0	0.00529	0.000109	0.677

TABLE 3.4: Results of the η'-pole contribution (2.28) using the $\mathcal{F}^{EVMD}_{\eta'\gamma^*\gamma^*}\left(q_1^2, q_2^2\right)$ form factor (2.50) as a function of a cut-off Λ in the loop momenta.

3.4 Pseudoscalar-pole contribution

The sum of the three light pseudoscalar poles (π^0, η, η') gives the pseudoscalar-pole contribution. Our estimations are

$$\begin{aligned} a_\mu^{LbL;PS} &= a_{\mu\ EVMD}^{LbL;\pi^0} + a_{\mu\ EVMD}^{LbL;\eta'} + a_{\mu\ EVMD}^{LbL;\eta'} \\ &= (6.2 \pm 1.2) \times 10^{-10} \end{aligned} \tag{3.20}$$

$$\begin{aligned} a_\mu^{LbL;PS} &= a_{\mu\ ELMD}^{LbL;\pi^0} + a_{\mu\ EVMD}^{LbL;\eta'} + a_{\mu\ EVMD}^{LbL;\eta'} \\ &= (7.3 \pm 1.2) \times 10^{-10} \end{aligned} \tag{3.21}$$

where we have used the EVMD and ELMD π^0-pole estimations respectively. The errors have been added linearly. In comparison, we give the value obtained by Knecht and Nyffeler [43]

$$\begin{aligned} a_\mu^{LbL;PS} &= a_{\mu\ LMD+V}^{LbL;\pi^0} + a_{\mu\ VMD}^{LbL;\eta'} + a_{\mu\ VMD}^{LbL;\eta'} \\ &= (8.3 \pm 1.2) \times 10^{-10} \end{aligned} \tag{3.22}$$

We also provide the results obtained from other references and methods (see Fig. 3.8). As observed, the values for the pseudoscalar (PS) contribution vary from 6×10^{-10} to 12×10^{-10}. The two reference values, which are most frequently used in the literature, are form the groups JN and PdRV,

$$a_\mu^{LbL;PS} = (9.9 \pm 1.6) \times 10^{-10} \tag{3.23}$$

$$a_\mu^{LbL;PS} = (11.4 \pm 1.3) \times 10^{-10} \tag{3.24}$$

Group	HLBL	π, K loop	PS	higher spin	quark loop	method
BPP [15]	+83(32)	−19(13)	+85(13)	−4(3)	+21(3)	ENJL, '95 '96 '02
HKS [16]	+90(15)	−5(8)	+83(6)	+1.7(1.7)	+10(11)	LHS, '95 '96 '02
KN [17]	+80(40)		+83(12)			Large N_c+χPT, '02
MV [18]	+136(25)	0(10)	+114(10)	+22(5)	0	Large N_c+χPT, '04
JN [8]	+116(40)	−19(13)†	+99(16)	+15(7)	+21(3)†	Large N_c+χPT, '09
PdRV [10]	+105(26)	−19(19)	+114(13)	+8(12)	0	Average, '09
HK [19]	+107		+107			Hologr. QCD, '09
DRZ [20]	+59(9)		+59(9)			Non-local q.m., '11
EMS [21–23]			+90(7)			Padé-data driven,'13
EMS [23,24]			+88(4)			Large N_c , '13
GLCR [25]			+105(5)			Large N_c+χPT, '14
J [26]				$+8(3)_{\text{axial}}$		Large N_c+χPT, '15
BR [27]		$-20(5)_{\pi\text{ only}}$				Large N_c+χPT, '16
MS [28]			+94(5)			Padé-data driven,'17
CHPS [29]		$-24(1)_{\pi\text{ only}}$				Disp Rel, '17

FIGURE 3.8: The HLbL and its different contributions from different references and methods, representing the progress on the field and the variety of approaches considered. † indicates used from a previous calculation. Units of 10^{-11}. Adapted from [49]. The references of the groups belong to [49].

Even though our estimations (3.20) and (3.21) fall within the range, they are clearly below the average. As mentioned before, our extended form factors are smaller than the non-extended versions. Consequently, our contributions are smaller too. Additionally, they do not show the asymptotic behaviour expected from experiments (3.10). Nevertheless, the Dual-QCD_∞ model has the flexibility of controlling this asymptotic behaviour with a single free parameter β. Then, it could be interesting for future work to update this parameter in order to obtain form factors more fitted to the experimental data. In fact, the parameter β used in our calculations is not updated and it does not represent accurately all radial excitations of the rho meson. Furthermore, the $\eta\gamma\gamma$ and $\eta'\gamma\gamma$ transition form factors were adapted from the $\pi^0\gamma\gamma$ form factor. In order to improve the results, a detailed short-distance analysis of these form factors in large-N_c QCD for non-zero quark masses should be performed, as done for the $\pi^0\gamma\gamma$ case.

In order to observe how our estimations affect the difference between the experimental value of the anomalous magnetic moment of the muon a_μ^{exp} (1.16) and its theoretical counterpart in the standard model a_μ^{SM} (Fig. 1.13), we complement our results with those from the "Glasgow consensus" (see PdRB group from Fig. 3.8). We obtain

$$a_{\mu\ EVMD}^{HLbL} = (5.3 \pm 2.5) \times 10^{-10} \tag{3.25}$$

$$a_{\mu\ ELMD}^{HLbL} = (6.4 \pm 2.5) \times 10^{-10} \tag{3.26}$$

where the errors have been added in quadrature. Then, considering the results from the other contributions of the SM (Fig. 1.13), we obtain

$$a_{\mu\ EVMD}^{SM} = (11659172.8 \pm 5.3) \times 10^{-10} \tag{3.27}$$

$$a_{\mu\ ELMD}^{SM} = (11659173.9 \pm 5.3) \times 10^{-10} \tag{3.28}$$

and we end up with the following discrepancies

$$\Delta a_\mu^{EVMD} = a_\mu^{\text{EXP}} - a_{\mu\ EVMD}^{\text{SM}} = (36.3 \pm 8.2) \times 10^{-10} \approx 4.4\sigma \tag{3.29}$$

$$\Delta a_\mu^{ELMD} = a_\mu^{\text{EXP}} - a_{\mu\ ELMD}^{\text{SM}} = (35.2 \pm 8.2) \times 10^{-10} \approx 4.3\sigma \tag{3.30}$$

These results substantially increase the discrepancy of $3-4\sigma$ between experiment and theory that is obtained from the most recent models and data. Although it is not yet a 5σ, it is a sign of New Physics more promising than before. The justification of this outcome is the increase in the difference between theory and experiment. However, there are still the theoretical uncertainties from HVP and HLbL that need to be better controlled to draw firm conclusions. Furthermore, the Dual-QCD_∞ model discussed in this thesis is still incomplete and requires future work to review the form factors again and to compute the remaining contributions of the HLbL scattering.

Chapter 4

Conclusions and future direction

In this thesis, we have evaluated the anomalous magnetic moment of the muon a_μ induced by the pseudoscalar-pole contribution to the hadronic light-by-light scattering using the Dual-QCD_∞ model. The a_μ^{exp} measured by the Brookhaven National Laboratory (BNL) E821 experiment represents an interesting but not yet conclusive 3.4σ discrepancy from the Standard Model prediction (a_μ^{SM}), which is a very promising signal of New Physics. Waiting for new results from the Fermilab E989 and J-PARC E34 experiments, we have proposed a different theoretical approach to the HLbL scattering.

As we have seen, due to the non-perturbative nature of QCD, the largest uncertainties in the SM prediction come from the leading hadronic contributions: the HVP and HLbL insertions. Unlike the HVP, the HLbL cannot be expressed in terms of experimental observables and requires knowledge of QCD at all energy scales. Since this is not known yet, one needs to rely on hadronic models to compute it. Using the large-N_c and the chiral counting, it was proposed to split the HLbL into a set of different contributions: pseudoscalar exchange (dominant), charged pion and kaon loops, quark loop, and higher-spin exchanges. The large-N_c approach however has at least two shortcomings: firstly, it is difficult to use experimental data in a large-N_c world. Secondly, calculations carried out in the large-N_c limit demand an infinite set of resonances. Dealing with such sum remains cumbersome, and to a large extent illusory, since the characteristics of these states (masses, couplings, etc.) are in general not known. The purpose of the Dual-QCD_∞ model that has been used in this thesis is to sum up all the infinite number of zero width resonances that appear in the large-N_c limit. In order to do so, the masses and couplings of the zero-width states are fixed so that the form factors become Euler Beta functions of the Veneziano type, involving one single free parameter β which controls their asymptotic power behaviour.

Among the different contributions to HLbL, we have focused on the pseudoscalar-pole contribution. Fortunately, this contribution corresponds to the lowest-mass part of the rank-four hadronic vacuum polarization tensor $\Pi_{\mu\nu\lambda\rho}$ that is leading in the large-N_c limit. We have computed this contribution using the model from Knecht and Nyffeler [43]. The resulting two-loop integrals are treated by first performing the angular integration analytically, using the method of Gegenbauer polynomials (hyperspherical approach), followed by a numerical evaluation of the remaining two-dimensional integration over the moduli of the Euclidean loop momenta. However, one needs a model for the transition form factor. We have used the Dual-QCD_∞ model as an extension of the VMD and LMD transition form factors. Our motivations for using this model have been the improved predictions of the radiative meson decay widths using the EVMD form factor over the VMD results, and the hypothesis that considering additional vector meson states should give a better approximation of the form factors.

The pseudoscalar-pole contribution is given by the sum of the three light pseudoscalar poles (π^0, η, η'). We have computed and discussed the three of them separately, although they had a similar behaviour. In each case, we have seen that the EVMD and ELMD form factors are smaller than the corresponding non-extended versions. Consequently, the contribution to a_μ is smaller too. Our estimations have been $a_{\mu\ EVMD}^{LbL;PS} = (6.2 \pm 1.2) \times 10^{-10}$ and $a_{\mu\ ELMD}^{LbL;PS} = (7.3 \pm 1.2) \times 10^{-10}$, which are clearly below the average. Complementing these results with those from the "Glasgow consensus" we have obtained the discrepancies $\Delta a_\mu^{EVMD} \approx 4.4\sigma$ and $\Delta a_\mu^{ELMD} \approx 4.3\sigma$, which substantially increase the discrepancy of $3-4\sigma$ between experiment and theory that has been obtained from the most recent models and data. Therefore, it is a sign of New Physics more promising than before.

Despite the results obtained, there is still much work to be done in order to complete and improve our predictions. On one hand, we have restricted our analysis in the pion-pole approximation, which takes the form factor on the pion mass shell such that it simplifies the calculations. However, the pion is not necessarily near the pole, i.e. it holds for off-shell pions as well. Then, not only seems reasonable to consider the general case (pseudoscalar-exchange) because it is more complete, but also because the pion-pole approach has been recently criticized. Since we only have focused in the pseudoscalar-pole contribution, we should leave for future work a complete discussion of the $\Pi_{\mu\nu\lambda\rho}$ in order to study the remaining contributions of the HLbL within a theoretical framework close to the one adopted here. Furthermore, the $\eta\gamma\gamma$ and $\eta'\gamma\gamma$ transition form factors were adapted from the $\pi^0\gamma\gamma$ form factor. In order to improve the results, a detailed short-distance analysis of these form factors in large-N_c QCD for non-zero quark masses should be performed, as done for the $\pi^0\gamma\gamma$ case. On the other hand, we have seen that the extended form factors deduced from the Dual-QCD_∞ model do not show the asymptotic behaviour expected from experiments. Nevertheless, the Dual-QCD_∞ model has the flexibility of controlling this asymptotic behaviour with a single free parameter β. Then, it could be interesting for future work to update this parameter in order to obtain form factors more fitted to the experimental data.

Bibliography

[1] Mehran Zahiri Abyaneh. "The Anatomy of the Pion Loop Hadronic Light by Light Scattering Contribution to the Muon Magnetic Anomaly". MA thesis. Lund U., Dept. Theor. Phys., 2012. arXiv: 1208.2554 [hep-ph]. URL: http://inspirehep.net/record/1127351/files/arXiv:1208.2554.pdf.

[2] S. Aghababaei, M. Haghighat, and I. Motie. "Muon anomalous magnetic moment in the standard model extension". In: *Phys. Rev.* D96 (2017), p. 115028. DOI: 10.1103/PhysRevD.96.115028. arXiv: 1712.09028 [hep-ph].

[3] Bernard Aubert et al. "Measurement of the gamma gamma* —¿ pi0 transition form factor". In: *Phys. Rev.* D80 (2009), p. 052002. DOI: 10.1103/PhysRevD.80.052002. arXiv: 0905.4778 [hep-ex].

[4] O. Balea et al. "Neutral strange particle production in pi- p, pi- n and pi- c interactions at 40 gev/c. bucharest-budapest-cracow-dubna-hanoi-sofia-tashkent-tbilisi- ulan bator collaboration". In: *Nucl. Phys.* B79 (1974), pp. 57–69. DOI: 10.1016/0550-3213(74)90179-5.

[5] R. Michael Barnett et al. "Review of particle physics. Particle Data Group". In: *Phys. Rev.* D54 (1996), pp. 320–330. DOI: 10.1103/PhysRevD.54.1.

[6] H. J. Behrend et al. "A Measurement of the pi0, eta and eta-prime electromagnetic form-factors". In: *Z. Phys.* C49 (1991), pp. 401–410. DOI: 10.1007/BF01549692.

[7] J. S. Bell and E. de Rafael. "Hadronic vacuum polarization and g(mu)-2". In: *Nucl. Phys.* B11 (1969), pp. 611–620. DOI: 10.1016/0550-3213(69)90250-8.

[8] J. Beringer et al. "Review of Particle Physics (RPP)". In: *Phys. Rev.* D86 (2012), p. 587. DOI: 10.1103/PhysRevD.86.010001.

[9] Johan Bijnens and Mehran Zahiri Abyaneh. "The hadronic light-by-light contribution to the muon anomalous magnetic moment and renormalization group for EFT". In: *EPJ Web Conf.* 37 (2012), p. 01007. DOI: 10.1051/epjconf/20123701007. arXiv: 1208.3548 [hep-ph].

[10] Johan Bijnens, Elisabetta Pallante, and Joaquim Prades. "Hadronic light by light contributions to the muon g-2 in the large N(c) limit". In: *Phys. Rev. Lett.* 75 (1995). [Erratum: Phys. Rev. Lett.75,3781(1995)], pp. 1447–1450. DOI: 10.1103/PhysRevLett.75.3781,10.1103/PhysRevLett.75.1447. arXiv: hep-ph/9505251 [hep-ph].

[11] Johan Bijnens, Elisabetta Pallante, and Joaquim Prades. "Analysis of the hadronic light by light contributions to the muon g-2". In: *Nucl. Phys.* B474 (1996), pp. 379–420. DOI: 10.1016/0550-3213(96)00288-X. arXiv: hep-ph/9511388 [hep-ph].

[12] Johan Bijnens and Johan Relefors. "Pion light-by-light contributions to the muon $g-2$". In: *JHEP* 09 (2016), p. 113. DOI: 10.1007/JHEP09(2016)113. arXiv: 1608.01454 [hep-ph].

[13] Johan Bijnens et al. "QCD short distance constraints and hadronic approximations". In: *JHEP* 04 (2003), p. 055. DOI: 10.1088/1126-6708/2003/04/055. arXiv: hep-ph/0304222 [hep-ph].

[14] T. Blum et al. "Calculation of the hadronic vacuum polarization contribution to the muon anomalous magnetic moment". In: *Phys. Rev. Lett.* 121.2 (2018), p. 022003. DOI: 10.1103/PhysRevLett.121.022003. arXiv: 1801.07224 [hep-lat].

[15] Stanley J. Brodsky and G. Peter Lepage. "Large Angle Two Photon Exclusive Channels in Quantum Chromodynamics". In: *Phys. Rev.* D24 (1981), p. 1808. DOI: 10.1103/PhysRevD.24.1808.

[16] R. A. Bryan, C. A. Dominguez, and B. J. VerWest. "A Model for Off-shell Form-factors and Application to NN Scattering". In: *Phys. Rev.* C22 (1980), pp. 160–166. DOI: 10.1103/PhysRevC.22.160.

[17] Andrzej Czarnecki, William J. Marciano, and Arkady Vainshtein. "Refinements in electroweak contributions to the muon anomalous magnetic moment". In: *Phys. Rev.* D67 (2003). [Erratum: Phys. Rev.D73,119901(2006)], p. 073006. DOI: 10.1103/PhysRevD.67.073006,10.1103/PhysRevD.73.119901. arXiv: hep-ph/0212229 [hep-ph].

[18] Achim Denig. "Measurement of the π^0, η, η' transition form factors at $BABAR$". In: *Nucl. Phys. Proc. Suppl.* 234 (2013), pp. 283–286. DOI: 10.1016/j.nuclphysbps.2012.12.032.

[19] C. A. Dominguez. "Determination of the πNN, $\pi N\Delta$ and $\pi\pi\rho$ Form-factors From Quasi Two-body Hadronic Reactions". In: *Phys. Rev.* C24 (1981), pp. 2611–2617. DOI: 10.1103/PhysRevC.24.2611.

[20] C. A. Dominguez. "Electromagnetic Form-factor of the Pion: Vector Mesons or Quarks?" In: *Phys. Rev.* D25 (1982), p. 3084. DOI: 10.1103/PhysRevD.25.3084.

[21] C. A. Dominguez. "Radiative Meson Decays in a Dual Model". In: *Phys. Rev.* D28 (1983), p. 2314. DOI: 10.1103/PhysRevD.28.2314.

[22] C. A. Dominguez. "Pion form-factor in large N(c) QCD". In: *Phys. Lett.* B512 (2001), pp. 331–334. DOI: 10.1016/S0370-2693(01)00576-7. arXiv: hep-ph/0102190 [hep-ph].

[23] C. A. Dominguez. "Electromagnetic Form Factors of Hadrons in Quantum Field Theories". In: *AIP Conf. Proc.* 1056 (2008), pp. 23–30. DOI: 10.1063/1.3013047. arXiv: 0806.3360 [hep-ph].

[24] C. A. Dominguez. "Electromagnetic Form Factors of Hadrons in Dual-Large N_c QCD". In: *AIP Conf. Proc.* 1361 (2011), pp. 182–186. DOI: 10.1063/1.3622697. arXiv: 1002.3720 [hep-ph].

[25] Kevin T. Engel and Michael J. Ramsey-Musolf. "The Muon Anomalous Magnetic Moment and the Pion Polarizability". In: *Phys. Lett.* B738 (2014), pp. 123–127. DOI: 10.1016/j.physletb.2014.09.006. arXiv: 1309.2225 [hep-ph].

[26] R. Escribano, P. Masjuan, and P. Sanchez-Puertas. "The η transition form factor from space- and time-like experimental data". In: *Eur. Phys. J.* C75.9 (2015), p. 414. DOI: 10.1140/epjc/s10052-015-3642-z. arXiv: 1504.07742 [hep-ph].

[27] Rafel Escribano et al. "η transition form factor from space- and timelike experimental data". In: *Phys. Rev.* D94.5 (2016), p. 054033. DOI: 10.1103/PhysRevD.94.054033. arXiv: 1512.07520 [hep-ph].

[28] J. Grange et al. "Muon (g-2) Technical Design Report". In: (2015). arXiv: 1501.06858 [physics.ins-det].

[29] Frederick Earl Gray Jr. "A Measurement of the anomalous magnetic moment of the positive muon with a precision of 0.7 parts per million". PhD thesis. Illinois U., Urbana, 2003. DOI: 10.2172/1419219. URL: http://lss.fnal.gov/cgi-bin/find_paper.pl?thesis-2003-54.

[30] Mario Greco. "Deep inelastic processes". In: *Nucl. Phys.* B63 (1973), pp. 398–412. DOI: 10.1016/0550-3213(73)90154-5.

[31] J. Gronberg et al. "Measurements of the meson - photon transition form-factors of light pseudoscalar mesons at large momentum transfer". In: *Phys. Rev.* D57 (1998), pp. 33–54. DOI: 10.1103/PhysRevD.57.33. arXiv: hep-ex/9707031 [hep-ex].

[32] A. Guevara, P. Roig, and J. J. Sanz-Cillero. "Pseudoscalar pole light-by-light contributions to the muon $(g-2)$ in Resonance Chiral Theory". In: *JHEP* 06 (2018), p. 160. DOI: 10.1007/JHEP06(2018)160. arXiv: 1803.08099 [hep-ph].

[33] Jan Haas. "pion loop contribution to the anomalous magnetic moment of the muon". MA thesis. Justus-Liebig-Universität Giessen, 2013. URL: https://www.uni-giessen.de/fbz/fb07/fachgebiete/physik/einrichtungen/theorie/inst/theses/master/masterjhaas_final.pdf.

[34] M. Hayakawa and T. Kinoshita. "Pseudoscalar pole terms in the hadronic light by light scattering contribution to muon g - 2". In: *Phys. Rev.* D57 (1998). [Erratum: Phys. Rev.D66,019902(2002)], pp. 465–477. DOI: 10.1103/PhysRevD.57.465,10.1103/PhysRevD.66.019902. arXiv: hep-ph/9708227 [hep-ph].

[35] M. Hayakawa, T. Kinoshita, and A. I. Sanda. "Hadronic light by light scattering effect on muon g-2". In: *Phys. Rev. Lett.* 75 (1995), pp. 790–793. DOI: 10.1103/PhysRevLett.75.790. arXiv: hep-ph/9503463 [hep-ph].

[36] M. Hayakawa, T. Kinoshita, and A. I. Sanda. "Hadronic light by light scattering contribution to muon g-2". In: *Phys. Rev.* D54 (1996), pp. 3137–3153. DOI: 10.1103/PhysRevD.54.3137. arXiv: hep-ph/9601310 [hep-ph].

[37] F. Jegerlehner. "Essentials of the Muon g-2". In: *Acta Phys. Polon.* B38 (2007), p. 3021. arXiv: hep-ph/0703125 [hep-ph].

[38] Fred Jegerlehner and Andreas Nyffeler. "The Muon g-2". In: *Phys. Rept.* 477 (2009), pp. 1–110. DOI: 10.1016/j.physrep.2009.04.003. arXiv: 0902.3360 [hep-ph].

[39] Friedrich Jegerlehner. "The anomalous magnetic moment of the muon". In: *Springer Tracts Mod. Phys.* 226 (2008), pp. 1–426. DOI: 10.1007/978-3-540-72634-0.

[40] Friedrich Jegerlehner. "The Anomalous Magnetic Moment of the Muon". In: *Springer Tracts Mod. Phys.* 274 (2017), pp. 1–693. DOI: 10.1007/978-3-319-63577-4.

[41] T. Kinoshita, B. Nizic, and Y. Okamoto. "Hadronic Contributions to the Anomalous Magnetic Moment of the Muon". In: *Phys. Rev.* D31 (1985), p. 2108. DOI: 10.1103/PhysRevD.31.2108.

[42] M. Knecht. "The Anomalous magnetic moment of the muon: A Theoretical introduction". In: *Lect. Notes Phys.* 629 (2004), pp. 37–84. DOI: 10.1007/978-3-540-44457-2_2. arXiv: hep-ph/0307239 [hep-ph].

[43] Marc Knecht and Andreas Nyffeler. "Hadronic light by light corrections to the muon g-2: The Pion pole contribution". In: *Phys. Rev.* D65 (2002), p. 073034. DOI: 10.1103/PhysRevD.65.073034. arXiv: hep-ph/0111058 [hep-ph].

[44] L. G. Landsberg. "Electromagnetic Decays of Light Mesons". In: *Phys. Rept.* 128 (1985), pp. 301–376. DOI: 10.1016/0370-1573(85)90129-2.

[45] P. Masjuan, S. Peris, and J. J. Sanz-Cillero. "Vector Meson Dominance as a first step in a systematic approximation: The Pion vector form-factor". In: *Phys. Rev.* D78 (2008), p. 074028. DOI: 10.1103/PhysRevD.78.074028. arXiv: 0807.4893 [hep-ph].

[46] Pere Masjuan. "$\gamma * \gamma \to \pi^0$ transition form factor at low-energies from a model-independent approach". In: *Phys. Rev.* D86 (2012), p. 094021. DOI: 10.1103/PhysRevD.86.094021. arXiv: 1206.2549 [hep-ph].

[47] Pere Masjuan and Enrique Ruiz Arriola. "Regge trajectories of Excited Baryons, quark-diquark models and quark-hadron duality". In: *Phys. Rev.* D96.5 (2017), p. 054006. DOI: 10.1103/PhysRevD.96.054006. arXiv: 1707.05650 [hep-ph].

[48] Pere Masjuan, Enrique Ruiz Arriola, and Wojciech Broniowski. "Systematics of radial and angular-momentum Regge trajectories of light non-strange $q\bar{q}$-states". In: *Phys. Rev.* D85 (2012), p. 094006. DOI: 10.1103/PhysRevD.85.094006. arXiv: 1203.4782 [hep-ph].

[49] Pere Masjuan and P. Sanchez-Puertas. "Status of hadronic light-by-light scattering and the muon $(g-2)$". In: *PoS* FPCP2017 (2017), p. 028. DOI: 10.22323/1.304.0028. arXiv: 1711.02551 [hep-ph].

[50] Pere Masjuan and Pablo Sanchez-Puertas. "Pseudoscalar-pole contribution to the $(g_\mu - 2)$: a rational approach". In: *Phys. Rev.* D95.5 (2017), p. 054026. DOI: 10.1103/PhysRevD.95.054026. arXiv: 1701.05829 [hep-ph].

[51] Kirill Melnikov and Arkady Vainshtein. "Hadronic light-by-light scattering contribution to the muon anomalous magnetic moment revisited". In: *Phys. Rev.* D70 (2004), p. 113006. DOI: 10.1103/PhysRevD.70.113006. arXiv: hep-ph/0312226 [hep-ph].

[52] Chris Michael, Konstantin Ottnad, and Carsten Urbach. "η and η' masses and decay constants from lattice QCD with $N_f = 2+1+1$ quark flavours". In: *PoS* LATTICE2013 (2014), p. 253. arXiv: 1311.5490 [hep-lat].

[53] James P. Miller, Eduardo de Rafael, and B. Lee Roberts. "Muon (g-2): Experiment and theory". In: *Rept. Prog. Phys.* 70 (2007), p. 795. DOI: 10.1088/0034-4885/70/5/R03. arXiv: hep-ph/0703049 [hep-ph].

[54] Dario Moricciani, KLOE-2, and BGO-OD Collaborations. "Hadronic Light-by-Light contribution to the muon anomalous magnetic moment". In: *Journal of Physics: Conference Series* 349.1 (2012), p. 012005. URL: http://stacks.iop.org/1742-6596/349/i=1/a=012005.

[55] B. M. K. Nefkens and J. W. Price. "The Neutral decay modes of the eta meson". In: *Phys. Scripta* T99 (2002), pp. 114–122. DOI: 10.1238/Physica.Topical.099a00114. arXiv: nucl-ex/0202008 [nucl-ex].

[56] Andreas Nyffeler. "Hadronic light-by-light scattering in the muon g-2: A New short-distance constraint on pion-exchange". In: *Phys. Rev.* D79 (2009), p. 073012. DOI: 10.1103/PhysRevD.79.073012. arXiv: 0901.1172 [hep-ph].

[57] Andreas Nyffeler. "Hadronic light-by-light scattering in the muon g-2". In: *International Workshop on e+e- Collisions from Phi to Psi (PHIPSI17) Mainz, Germany, June 26-29, 2017*. 2017. arXiv: 1710.09742 [hep-ph]. URL: http://inspirehep.net/record/1632784/files/arXiv:1710.09742.pdf.

[58] Vladyslav Pauk. "Light-by-light scattering and muon's anomalous magnetic moment". In: (2014).

[59] Fredrik Perrsson. "Effects of different form-factors in meson photon photon transitions and the muon anomalous magnetic moment". MA thesis. Lund U., Dept. Theor. Phys., 1999. arXiv: hep-ph/0106130 [hep-ph].

[60] V. A. Petrov. "On Vector Dominance". In: *Mod. Phys. Lett.* A30.31 (2015), p. 1550164. DOI: 10.1142/S0217732315501643. arXiv: 1312.5500 [hep-ph].

[61] Joaquim Prades, Eduardo de Rafael, and Arkady Vainshtein. "The Hadronic Light-by-Light Scattering Contribution to the Muon and Electron Anomalous Magnetic Moments". In: *Adv. Ser. Direct. High Energy Phys.* 20 (2009), pp. 303–317. DOI: 10.1142/9789814271844_0009. arXiv: 0901.0306 [hep-ph].

[62] Enrique Ruiz Arriola and Wojciech Broniowski. "Pion transition form factor and distribution amplitudes in large-N(c) Regge model". In: *Phys. Rev.* D74 (2006), p. 034008. DOI: 10.1103/PhysRevD.74.034008. arXiv: hep-ph/0605318 [hep-ph].

[63] Enrique Ruiz Arriola and Wojciech Broniowski. "Pion transition form factor in the Regge approach and incomplete vector-meson dominance". In: *Phys. Rev.* D81 (2010), p. 094021. DOI: 10.1103/PhysRevD.81.094021. arXiv: 1004.0837 [hep-ph].

[64] Mitja Šadl. "The Anomalous Magnetic Moment of the Muon". In: (2017).

[65] Naohito Saito. "A novel precision measurement of muon g - 2 and EDM at J-PARC". In: *AIP Conference Proceedings* 1467.1 (2012), pp. 45–56. DOI: 10.1063/1.4742078. eprint: https://aip.scitation.org/doi/pdf/10.1063/1.4742078. URL: https://aip.scitation.org/doi/abs/10.1063/1.4742078.

[66] A. V. Samsonov. "Decay constant of the eta meson from QCD sum rule". In: (1998). arXiv: hep-ph/9807429 [hep-ph].

[67] M. Shifman and Boris Ioffe, eds. *At the frontier of particle physics. Handbook of QCD. Vol. 1-3*. Singapore, Singapore: World Scientific, 2001, pp. 507–568. ISBN: 9789810244453, 9789814492225. DOI: 10.1142/4544. URL: http://www.slac.stanford.edu/spires/find/books/www?cl=QCD161:S51:2001.

[68] Peter Stoffer et al. "Hadronic light-by-light scattering and the muon g2". In: *Nuovo Cim.* C38.4 (2016), p. 135. DOI: 10.1393/ncc/i2015-15135-9.

[69] M. Suzuki. "Pseudoscalar-Meson Decay Constants". In: (2004).

[70] M. Tanabashi et al. "Review of Particle Physics". In: *Phys. Rev. D* 98 (3 2018), p. 030001. DOI: 10.1103/PhysRevD.98.030001. URL: https://link.aps.org/doi/10.1103/PhysRevD.98.030001.

[71] S. Uehara et al. "Measurement of $\gamma\gamma^* \to \pi^0$ transition form factor at Belle". In: *Phys. Rev.* D86 (2012), p. 092007. DOI: 10.1103/PhysRevD.86.092007. arXiv: 1205.3249 [hep-ex].

[72] G. Veneziano. "An Introduction to Dual Models of Strong Interactions and Their Physical Motivations". In: *Phys. Rept.* 9 (1974), pp. 199–242. DOI: 10.1016/0370-1573(74)90027-1.